A DYNAMICS MODEL OF THE COAXIAL FLOW GASEOUS CORE NUCLEAR REACTOR SYSTEM

A THESIS

Presented to

The Faculty of the Graduate Division

by

Kyle H. Turner, Jr.

In Partial Fulfillment

of the Requirements for the Degree

Doctor of Philosophy

in the School of Nuclear Engineering

Georgia Institute of Technology

December, 1971

In presenting the dissertation as a partial fulfillment of the requirements for an advanced degree from the Georgia Institute of Technology, I agree that the Library of the Institute shall make it available for inspection and circulation in accordance with its regulations governing materials of this type. I agree that permission to copy from, or to publish from, this dissertation may be granted by the professor under whose direction it was written, or, in his absence, by the Dean of the Graduate Division when such copying or publication is solely for scholarly purposes and does not involve potential financial gain. It is understood that any copying from, or publication of, this dissertation which involves potential financial gain will not be allowed without written permission.

7/25/68

A DYNAMICS MODEL OF THE COAXIAL FLOW GASEOUS CORE NUCLEAR REACTOR SYSTEM

Approved:

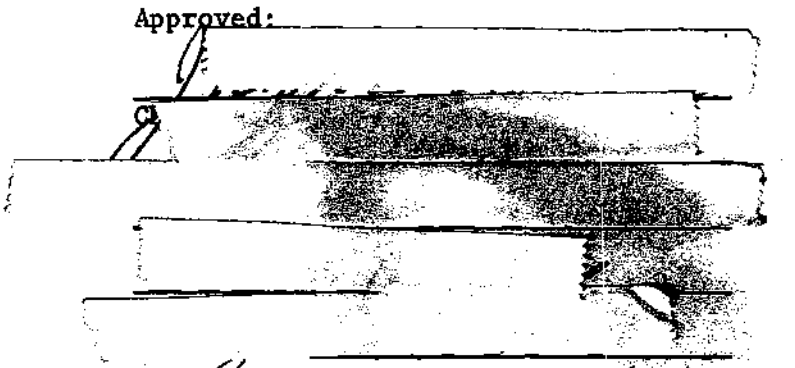

Date approved by Chairman: 11/12/71

ACKNOWLEDGMENTS

I am especially grateful to my thesis advisor, Dr. Joseph D. Clement, whose assistance, encouragement, and guidance made the completion of this research possible. Dr. W. Waverly Graham, III, Dr. J. Richard Williams, and Dr. James C. Wu deserve special thanks as members of my thesis committee and for the invaluable professional support they provided. Mr. Robert G. Ragsdale, also a thesis committee member, has given unselfishly of his time and knowledge in providing the specifications of the reference design and information required for the development of the model.

Mr. Albert F. Kascak and Mr. Robert E. Hyland, Mr. Ragsdale's coworkers at the NASA-Lewis Research Center, are due thanks for their advice and interest.

I would like to thank my fellow students Dr. William R. Jacobs, Mr. Robert A. Benns, and Mr. Steven D. Thompson for their constant sympathetic ear and help.

To my parents, I express my sincere appreciation for their continuing support and encouragement. Finally, and most importantly, I would like to express to my wife Carol my deep appreciation for her love and understanding throughout the duration of this effort.

TABLE OF CONTENTS

TABLE OF CONTENTS (Concluded)

LIST OF TABLES

LIST OF ILLUSTRATIONS

LIST OF ILLUSTRATIONS (Concluded)

SUMMARY

A mathematical model has been derived for the coaxial flow gaseous core nuclear reactor system which has been proposed by Ragsdale and his co-workers at the NASA-Lewis Research Center. The equations were derived from elementary neutron, heat, and mass balances on the components of the system and from correlations presented in the work of Ragsdale, Parks and Lane, and Patch. Propellant flow out of the reactor cavity was assumed to be governed by the choked-flow equation. The net radiant heat transfer between the fuel and propellant was calculated by defining effective black-body radiating temperatures which yield the correct heat fluxes at normal operating conditions. Average properties were assumed to sufficiently describe the state of the reactor; no spatial variations were taken into account. Reactivity mechanisms which were considered included changes in fuel mass, fuel temperature, fuel cloud radius, propellant density, propellant temperature, and moderator temperature.

The system response for positive reactivity insertions, perturbations in the propellant and fuel flow rates at the cavity inlet, and for termination of the moderator primary coolant flow has been predicted. The predictions indicate that the reactor is not inherently stable, but the response to positive reactivity insertions is considerably more sluggish than for an equivalent system with no reactivity feedback. Decreases in propellant flow rate at the cavity inlet resulted in a fairly rapid power increase whereas termination of the fuel injection and moderator

primary coolant flow rate caused a reactor shutdown. For all the cases in which the power level rose, the time scale for the reactor to reach conditions which might cause system damage is long enough so that present control technology can be invoked to control the reactor.

The model is slightly sensitive to variations in the propellant and fuel temperature coefficients of reactivity and quite sensitive to variations in the propellant density and fuel cloud radius coefficients. Changes in fuel mass and moderator temperature coefficients have virtually no effect on the model. Changing the rate at which fuel is lost as the fuel volume fraction increases also does not affect the model's predictions.

The best of the proposed control systems seems to be the concept of control drums in the moderator region. Regulation of the fuel injection rate does not give reactivity insertions fast enough to limit most transients, and regulation of the propellant injection rate was found to be good only for shutdown of the reactor--any change in propellant inlet flow rate introduces fairly large changes in reactivity.

CHAPTER I

INTRODUCTION

The Gaseous Core Nuclear Reactor

The gaseous core nuclear reactor was originally conceived in the process of searching for a better means of rocket propulsion for long range space missions. The two parameters of primary importance in evaluating the suitability of a given propulsion system are the specific impulse and the thrust-to-weight ratio.[1] The latter parameter is, of course, the thrust of the engine divided by the total vehicle weight; the specific impulse I_{sp} is defined by

$$I_{sp} = \frac{\text{Engine Thrust}}{\dot{m}\, g_c}$$

where $\dot{m}$ is the mass flow rate of the propellant and g_c is the gravitational acceleration at sea level. If m_i and m_f are the initial and final mass of a rocket which has executed a mission equivalent to a velocity change Δv in free space, the relation

$$m_i/m_f = e^{\frac{\Delta v}{v_e}} \qquad (1\text{-}1)$$

where v_e is the propellant exhaust velocity,

holds. Since the thrust is given by $\dot{m}\, v_e$, equation (1-1) may be written

$$m_i/m_f = e^{\frac{\Delta v}{g_c I_{sp}}} \qquad (1\text{-}2)$$

from which it may be seen that an increase in I_{sp} may cause a dramatic decrease in the size of a vehicle required to accomplish a given mission. Today's chemical rockets produce a specific impulse of about 500 seconds, and the solid core nuclear rocket is expected to eventually yield an I_{sp} of 1000 sec.[2] In designs currently being studied, the gaseous-core nuclear rocket is expected to produce an I_{sp} of 5000 sec.[3] Thus, the elimination of the fuel temperature restraints inherent in the solid core allows much higher propulsion levels.

The gaseous core nuclear reactor is based on the concept of a fissioning uranium plasma transferring heat radiatively to a hot gas which serves as the working fluid. Two types of gas-core reactors are currently under study; they are (1) the closed cycle or nuclear light bulb and (2) the coaxial flow reactor. The nuclear light bulb concept involves containing the uranium plasma by a thin transparent wall through which the thermal radiation passes to heat the working fluid. This basic concept is shown in Figure 1 and is being studied at the United Aircraft Research Laboratory. The coaxial-flow reactor utilizes a slow moving central stream of gaseous fissioning fuel to radiatively heat a more rapidly moving annular stream of particle-seeded gas which serves as the working fluid. Figure 2 is a diagram of a coaxial-flow reactor system which is being investigated by researchers at the NASA-Lewis Research Center. The original work on the coaxial flow reactor was performed by Rom[4] (who obtained a patent) and Ragsdale[5,6] and they have directed extensive studies

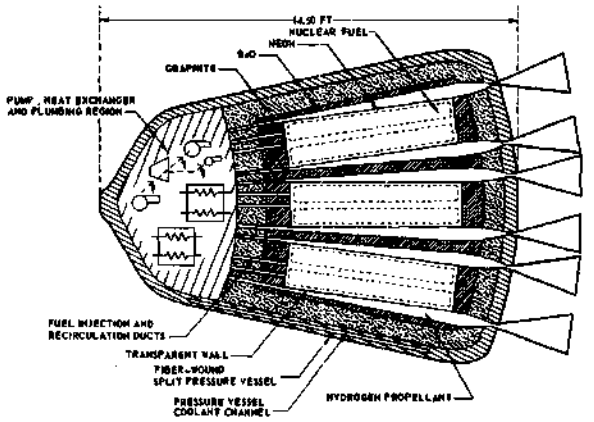

Figure 1. Schematic of the Nuclear Light Bulb Gaseous Core Reactor Concept

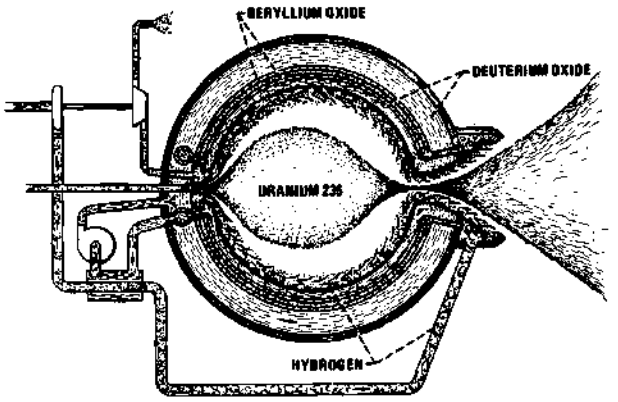

Figure 2. Conceptual Coaxial Flow Gaseous Core Reactor System

of this concept over the past 10 years. McLafferty[7] obtained the first patent on the nuclear light bulb concept which has been examined also during the past decade.[8,9]

Recently, the increasing concern over thermal and other forms of environmental pollution has led to the search for more efficient terrestrial power generation systems. Magnetohydrodynamic (MHD) generation has shown some promise, but there has been a lack of suitable heat sources. The gaseous core reactor seems to fill this gap perfectly. In fact, Rosa states that the gas core reactor may very well prevent MHD technology from becoming obsolete.[10] Several design studies of gas-core MHD power plants and propulsion systems have been reported.[10-14] One study[14] concluded that large commercial power plants using a gas core nuclear rocket type reactor might have thermal efficiencies as high as 70 percent. Other advantages include very high fuel economy and the reduction of thermal pollution per electrical megawatt by a factor of three to five over today's plants.

In addition to these applications, a gaseous core form of the fast breeder reactor has been proposed.[15] This study, by Kallfelz and Williams, used a one-dimensional diffusion theory code to study the effects on criticality of various fuel and blanket radii.

Studies in Rocket Reactor Dynamics

Solid Core

There has been a great deal of theoretical and experimental work done on system and reactor dynamics for solid core nuclear rocket engine designs. One of the most comprehensive of the theoretical analyses has been done by Esposito,[16] who examined the system dynamics of the Nerva

reactor.

Esposito's approach was to write the equations describing each facet of the system, i.e., reactor kinetics, heat generation and transfer, and fluid flow, discretize them in time and in the spatial coordinates, and couple the resulting models of the individual systems to obtain an overall system model. The form of these equations that the author used to arrive at his model was as follows:

Conservation of Mass (continuity)

$$\frac{\partial \rho}{\partial t} + \frac{\partial}{\partial z} (\rho u_z) = 0 \qquad (1\text{-}3)$$

where u_z is the local fluid velocity in the z-direction and ρ is the local fluid density.

Conservation of Energy

$$\frac{\partial}{\partial t}\left[\rho(U + u^2/2gJ)\right] + \frac{\partial}{\partial z}\left[\rho u_z(U + u^2/2gJ)\right] - \frac{1}{J}\frac{\partial}{\partial z}(Pu_z) = 4q_w/D \qquad (1\text{-}4)$$

where U = internal energy

u = local fluid velocity

g = gravitational constant

J = Joule's constant

P = static pressure

q_w = wall heat flux

D = flow diameter for propellant

Conservation of Momentum

$$\frac{\partial P}{\partial z} = -\frac{\rho}{g}\frac{\partial u_z}{\partial t} - \frac{u_z \rho}{g}\frac{\partial u_z}{\partial z} - \frac{4}{D}\left(f\,\frac{\rho u_z^2}{2g}\right) \tag{1-5}$$

where f is a correlating friction factor.

Neutron Kinetics Equations

$$\frac{dN(t)}{dt} = \left(\frac{\delta k(t)-\beta}{\ell}\right) k_{eff} N(t) + \Sigma\, \lambda_i C_i(t) \tag{1-6}$$

and

$$\frac{dC_i(t)}{dt} = \frac{\beta_i N(t)}{\ell}\, k_{eff} - \lambda_i C_i(t) \tag{1-7}$$

Esposito used this model to predict temperature distributions, pressure levels, and power level for various perturbations from steady state conditions and for the reactor startup sequence.

Gaseous Core

There have been no detailed studies made to model and/or study the dynamic behavior of coaxial flow gaseous core reactors. Latham, Bauer, and Rodgers,[17,18] however, have examined system stability for the nuclear light bulb engine at United Aircraft Corporation. They also utilized finite-difference approximations of the thermal, fluid dynamics, and neutron kinetics equations. These equations were, however, based on the assumption that the time behavior of a characteristic of a given component is proportional to the percentage change in power level rather than being derived from the "standard" balance equations as done by Esposito. For instance, the temperature rise in a given component following an increase in power would be written

$$\Delta T = (\Delta T)_o \left(1 + \sum_{i=1}^{\frac{\tau_R}{\Delta t}} \frac{\delta P}{P_o} \frac{\Delta t}{\tau_R}\right) \qquad (1\text{-}8)$$

where

ΔT = temperature difference at any time t

$(\Delta T)_o$ = steady state temperature difference

Δt = time increment

τ_R = residence time in component

$\delta P/P_o$ = percentage change in power (current value of power perturbation divided by steady state power)

Equations describing turbine and pump requirements, heat deposition in the transparent wall, reactivity coefficients, and neon buffer flow required to protect the wall were taken from other work.[19-22] Results from these studies included predicting the response of the reactor system to perturbations in several of the parameters describing the condition of the system and evaluating the suitability of a number of proposed control systems.

Conclusions that the authors were able to draw from their work included:

1. No unacceptable thermal stresses would be encountered during startup.

2. All perturbations resulted in damped oscillatory variations in the other engine parameters.

3. Reactor control could be effectively accomplished by regulation of the fuel injection rate.

Cavity Reactor Experiments

For several years, critical experiments were carried out at the low power test facility in Idaho by the General Electric Company.[23-27] All of the experiments were conducted to simulate, in some form, the geometry of the coaxial flow gas-core reactor. Only a few of the results obtained are directly applicable to dynamics of the reactor system. Pincock and Kunze[23] describe the measurement of a reflector temperature coefficient of reactivity for a simple cylindrical configuration 121.92 cm long and 182.88 cm in diameter surrounded by an 88.90 cm thick D_2O region.

One group of experiments[27] was devoted to the measurement of the reactivity effects of fuel waves being formed by the flow regime of the cavity. These measurements were made by comparing the system's reactivity with simulated waves to reactivities measured in the "smooth" cylindrical geometry described above. Two major wave configurations were investigated; their description, along with their maximum effect on reactivity, are shown below.

1. Wave crest develops, giving a net fuel addition to the core
   a) 7.3 cm crest + 0.7% Δk
   b) 22.0 cm crest + 6 % Δk
2. Wave crest and trough develops, with no net fuel addition to the core
   a) 7.3 cm amplitude + 0.3% Δk
   b) 22.0 cm amplitude + 2.8% Δk

In addition, the data showed that the worth of the fuel wave did not change appreciably as the wave progressed down the length of the core.

In addition to these wave measurements, two control methods were investigated. These consisted of 1) a cadmium sleeve to be moved longitudinally so as to encircle the core radially and 2) a system of rotating control drums in the reflector region. Both systems were found to incorporate at least -10% Δk in reactivity, which was adequate to shut down the reactor.

Purpose of This Research

Knowledge of a reactor system's behavior in the non-steady state is of primary importance in designing and building any type of nuclear power plant. The purpose of the research described in this thesis was to develop a mathematical model of the coaxial flow gaseous core nuclear reactor system. The model was designed to:

1. Determine the system's response to perturbations in parameters describing the state of the system.
2. Evaluate the suitability of several proposed control systems.
3. Determine the sensitivity of the response to variations in the equations describing the processes taking place in the system in order to indicate the areas in which further research is required to more accurately model the reactor.

Description of the Reference System

The physical layout of the coaxial flow gaseous core nuclear rocket engine which is studied in this research is shown in Figure 3. Uranium fuel is fed into the reactor cavity in solid form where it is vaporized and contained by a faster-moving stream of hydrogen propellant gas flowing coaxially around the central fuel cloud. The walls of the cavity are made

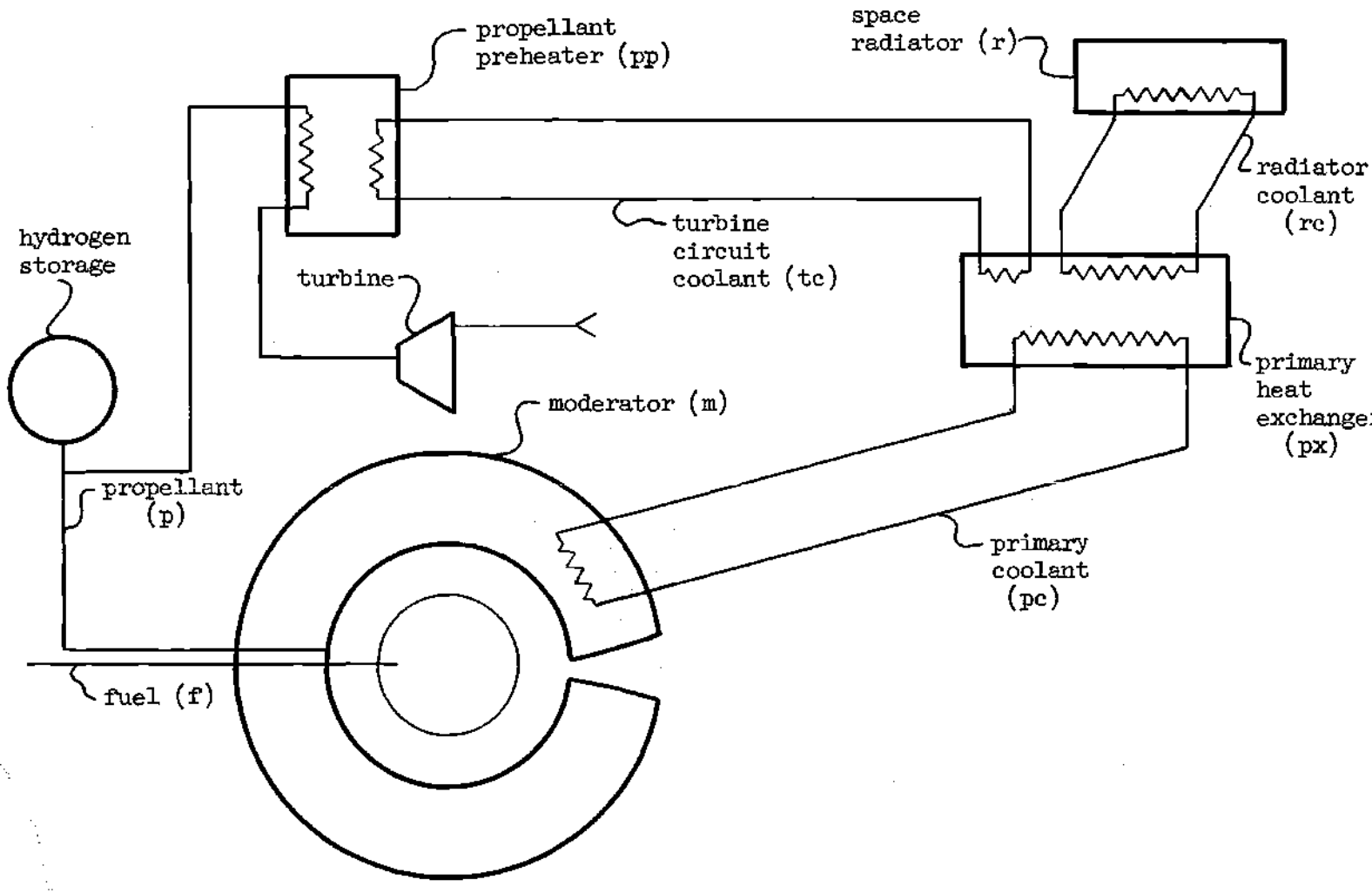

Figure 3. Schematic of the Reference Coaxial Flow Gaseous Core Reactor System Studied in This Research

of a porous material so that the propellant may be introduced uniformly over the inner surface, thus providing better fuel containment and helping to limit the wall temperature to a reasonable value. The propellant is heated by thermal radiation from the fissioning fuel cloud and is expelled through the exhaust nozzle producing the engine thrust. Since the propellant at its cavity entrance temperature is essentially transparent to the radiation being emitted from the fuel cloud, the hydrogen must be seeded with small particles which render the mixture entering the cavity opaque to radiant energy and thereby prevent any significant heat flux from reaching the cavity walls. That fraction of the energy produced in the fuel which is not emitted as thermal radiation is released in the form of gamma rays and neutrons which deposit heat in the moderator. The moderator rejects heat to the helium primary coolant which, in turn, rejects heat to the space radiator and turbine circuits via the primary heat exchanger. Most of the energy deposited in the moderator by gamma ray absorption and neutron slowing down is conveyed to the space radiator where it is dumped into space; the remainder of the heat is used to operate a turbine and generate power. The fuel is fully enriched uranium 235, the propellant is hydrogen seeded with tungsten (0.2% by weight), and the moderator is beryllium oxide. Both secondary working fluids are liquid sodium.

Robert G. Ragsdale and his co-workers at the NASA-Lewis Research Center have determined most of the nominal steady state operating conditions for the system presented in Figure 3. These conditions are listed in Table 1. The design of the moderator cooling system has not been

Table 1. Nominal Steady State Operating Conditions for the Reference Coaxial Flow Gaseous Core Reactor

Reactor Power	5900 megawatts
Engine Thrust	44,000 pounds
Specific Impulse	4400 seconds
Cavity Pressure	400 atmospheres
Average Fuel Temperature	90,000°R
Average Propellant Temperature	26,000°R
Fuel Cloud Diameter	6.7 feet
Fuel Mass (U-235)	60 pounds
Propellant Mass Flow Rate (cavity exit)	10 pounds/second
Fuel Mass Flow Rate (cavity exit)	.05 pounds/second
Moderator Temperature	2500°R
Space Radiator Temperature	2000°R

completed, and, for the purposes of deriving a dynamics model of this system, a set of consistent temperatures was arbitrarily chosen which describes the state of the heat removal loops during steady state operation. Figure 4 specifies the assumed nominal operating conditions of the cooling circuits.

The steady state operating conditions summarized in Table 1 were found from detailed heat transfer and neutronics calculations and from fluid mechanics experiments. The heat transfer analysis[28,29] was based on the best current estimates of the uranium and hydrogen properties at the operating temperatures and pressures. Detailed nuclear calculations[30] were made to find the mass of uranium which must be contained in the cavity in order to produce a critical system. The flow experiments[31,32] were conducted to insure that the degree of fuel containment required can, in fact, be obtained.

The nominal operating conditions assumed in this analysis are not the only values at which a reactor of this type might operate; rather they are one set of an entire spectrum of reference designs that have been studied. The variation of the characteristics of a given configuration basically involves a compromise between advantages and drawbacks. For instance, the thrust can be increased by increasing the uranium loss rate or by increasing the cavity pressure, which requires a stronger (and therefore heavier) pressure shell. The critical mass required can be decreased by increasing the moderator size, but this modification would result in a significant increase in weight. The essential point to be recognized about the listed operating conditions is that they represent

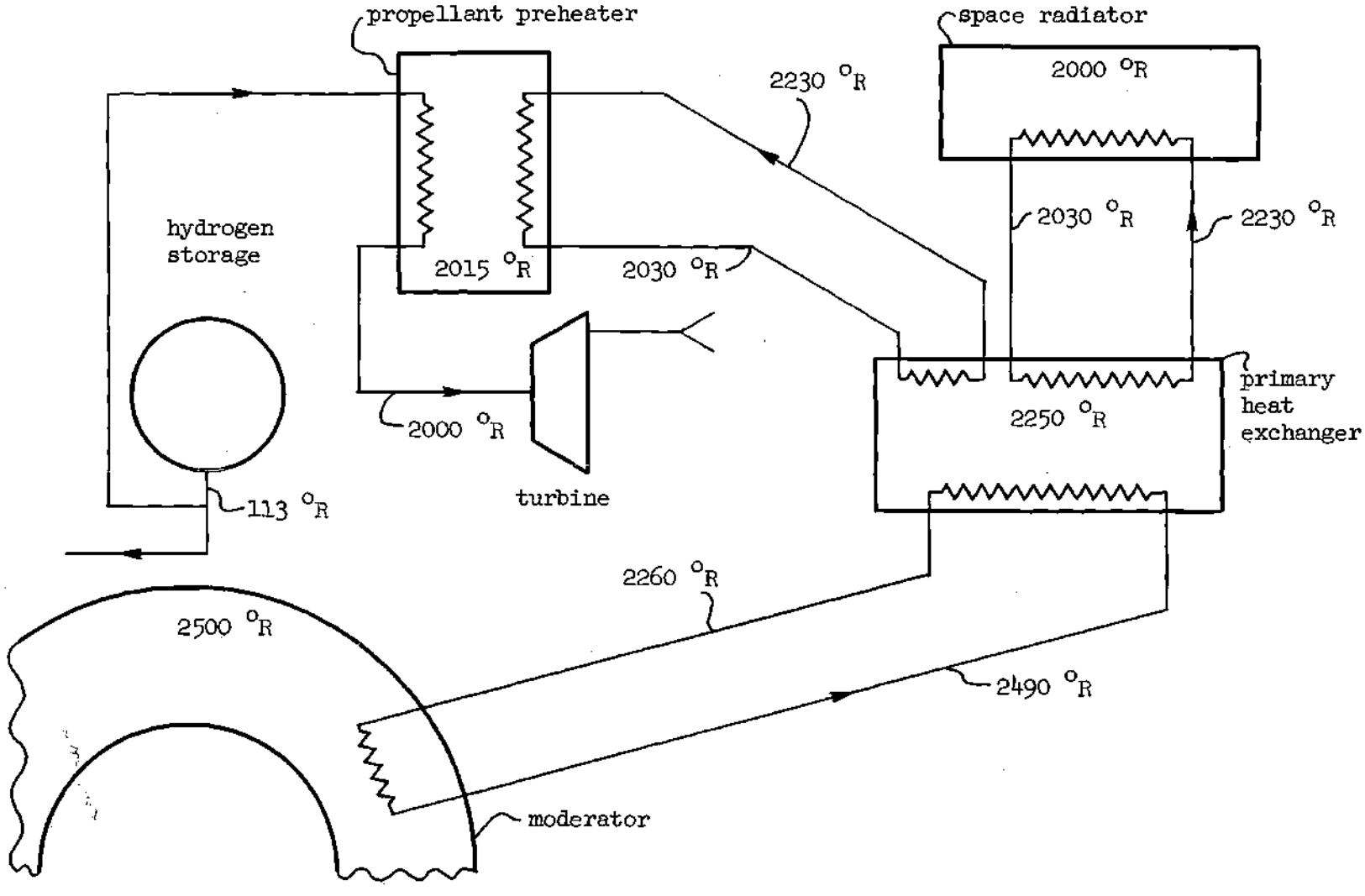

Figure 4. Initial Conditions in the Moderator Cooling System

one of a group of consistent steady state parameter values which describe a reactor system whose thrust and specific impulse are high enough to be of practical interest as a means of rocket propulsion.

CHAPTER II

DERIVATION OF THE DYNAMICS MODEL

To construct a mathematical model of a physical system, it is first necessary to write a system of equations which describe the dynamic behavior of the quantities which specify the state of the system at any given time. These equations are obtained by finding the relationships which describe the physical processes taking place in the system. This chapter is devoted to the derivation of the equations governing the dynamic behavior of the coaxial flow gaseous core nuclear reactor. A list of the symbols used in this discussion appears in Appendix A.

Neutron Kinetics Model

If it is assumed that the neutronics characteristics of the reactor can be adequately described by the average neutron density n, i.e., if the spatial and energy dependence of n are neglected, the dynamic behavior of n can be described by

$$\frac{dn}{dt} = \left(\frac{\rho - \beta_{eff}}{\ell}\right) n + \sum_i \lambda_i C_i \qquad (2\text{-}1)$$

where ρ is the reactivity, defined by $(k-1)/k$ where k is the number of neutrons produced in one generation divided by the number of neutrons produced in the previous generation, ℓ is the average neutron lifetime, β_{eff} is the effective delayed neutron fraction, C_i is the concentration of the

i^{th} delayed neutron precursor, and λ_i is the decay constant of the i^{th} delayed group. The behavior of the concentration of the i^{th} delayed neutron precursor is governed by

$$\frac{dC_i}{dt} = \frac{\beta_i}{\ell} n - (\lambda_i + \lambda_f) C_i \tag{2-2}$$

where λ_f is the reciprocal of the fuel residence time and β_i is the fraction of the delayed neutrons in the i^{th} group.

The parameter β_{eff} appearing in equation (2-1) differs from the total delayed neutron fraction $\beta (= \Sigma \beta_i)$ because, in the coaxial flow gaseous core reactor, some delayed neutron precursors may be lost from the core before decaying, thus reducing the number of delayed neutrons produced per fission. The relationship between β_{eff} and β can be found by examining equations (2-1) and (2-2) for the condition of zero derivatives. In the steady state, equation (2-2) may be solved for C_i yielding

$$C_i = \frac{\beta_i n}{\ell(\lambda_i + \lambda_F)} \tag{2-3}$$

This result may then be substituted into equation (2-1) with $\frac{dn}{dt} = \rho = 0$; solving the resulting relation for β_{eff} yields

$$\beta_{eff} = \sum_i \frac{\beta_i \lambda_i}{\lambda_i + \lambda_F}$$

which indicates, as expected, that the fraction of delayed neutrons contributing to the overall neutron population is reduced when the loss rate of precursors due to fuel flow is increased. The value of β_{eff} for the

reference system was 6.45×10^{-3}.

The term β_{eff} refers to the fraction of fissions caused by delayed neutrons. It is not, in general, equal to β, the delayed neutron fraction, because the delayed neutrons are born with an average energy of several hundred keV, considerably less than the average birth energy of 2 MeV of the prompt neutrons. β_{eff} may be larger than β, as in the case of reactors fueled with fully enriched uranium where the prompt neutrons have a larger chance than the delayed neutrons to escape from the system or be absorbed without causing fissions. For reactors with lightly enriched fuel, β_{eff} may be smaller than β because the prompt neutrons will cause fast fissions in the U-238. It is expected that the difference in average birth energy of prompt and delayed neutrons would cause an increase in the delayed neutron fraction for the concept under study. However, in the absence of a calculation of the effect of this energy difference on β, it was assumed, for the purposes of this study, that the delayed neutrons were born at the same average energy as the prompt neutrons. Thus, β_{eff}, as used here, reflects only the loss of delayed neutron precursors by flow out of the reactor cavity.

Cavity Fluid Dynamics and Heat Transfer

If it is assumed that the average fuel temperature T_f may be used to describe the heat transfer properties of the fuel, a differential equation governing the dynamic behavior of T_f may be derived from a heat balance of the form

heat accumulation rate = heat generation rate - heat removal rate. (2-5)

The rate of heat accumulation in the fuel is given by $m_f C_f \frac{dT_f}{dt}$ where m_f is the mass of fuel in the cavity and C_f is its specific heat. There are two mechanisms of heat loss which remove energy from the fuel cloud: radiative transfer to the propellant and neutron and gamma ray heating to the moderator. Heat gain occurs through absorption of the energy released by fissions in the fuel; the net rate of introduction of heat into the fuel is equal to the reactor power.

The net radiant heat flux between two bodies which are at uniform temperature is given by

$$q_{rad} = \xi \sigma (T_h^4 - T_c^4) \qquad (2\text{-}6)$$

where T_h is the temperature of the hotter body, T_c is the temperature of the cold body, σ is the Stefan-Boltzmann constant, and ξ is a factor which accounts for the relative geometries and emissivities of the two bodies. Implicit in the use of equation (2-6) is the assumption that the two bodies are at uniform temperatures, i.e., that the radiation from each body is characterized by a single average temperature. The analysis of radiant heat transfer between gases presents a more difficult problem than is indicated by the form of equation (2-6) because the energy emitted and the opacities of the gases are both dependent on the radiation wavelength and the gas temperature. In addition, the propellant and fuel gases do not interact as separate bodies; in general, every point in one region may interact with every point in the other. Thus, an exact representation of the radiant heat transfer rates between the two gases would require a knowledge of the spatial temperature distribution in each region.

However, by assuming that the fuel and propellant gases are grey, that is, that the opacities are not functions of the radiation wavelength, an equation similar in form to equation (2-6) can be used to represent the net radiant heat flux from the fuel to the propellant. The development of this equation is performed as follows.

Ragsdale and Kascak[33] have derived analytical expressions for the temperature distribution in the fuel for several fuel cloud geometries. The results of the derivation for a spherical geometry can be written

$$\frac{T}{T_b} = \left[\frac{1}{2}\left(1 + \frac{3}{kr_f}\right) + \frac{3kr_f}{16}\left(1 - \left(\frac{r}{r_f}\right)^2\right)\right]^{\frac{1}{4}} \qquad (2\text{-}7)$$

where T is the temperature at point r, T_b is the brightness temperature (explained below), k is the linear absorption coefficient of the fuel, and r is the distance from the center of the fuel cloud. The brightness temperature is defined by equating σT_b to the edge heat flux q_e; the edge heat flux is, in turn, found from a heat balance on the outermost fuel cloud layer. Since this expression holds for the temperature at every point in the fuel, it also holds for the average temperature; rewriting the equation for $T = T_f$ and letting $\bar{r}$ denote the radius at which the average temperature occurs yields

$$\frac{T_f}{T_b} = \left[\frac{1}{2}\left(1 + \frac{3}{kr_f}\right) + \frac{3kr_f}{16}\left(1 - \left(\frac{\bar{r}}{r_f}\right)^2\right)\right]^{\frac{1}{4}} . \qquad (2\text{-}8)$$

From this expression, it can be seen that the relationship between the average and brightness temperatures is linear only if the absorption coefficient is a constant. The work by Parks and Lane[34] has indicated that

the absorption coefficient for uranium is, however, a fairly strong function of temperature so that the shape of the temperature distribution changes with changing power generation levels. Thus, the brightness temperature cannot be linearly related to the average temperature during a reactor transient if the fuel absorption coefficient changes significantly. Work done by Kascak[35] in calculating the temperature distribution in the propellant region coupled with the results of Patch's calculations of hydrogen properties[36] indicate that a similar conclusion can be drawn concerning the relationship between the propellant average and brightness temperature.

For conditions not differing greatly from steady state, i.e., for perturbations which do not result in a significant change in the fuel and propellant absorption coefficients, a relation describing the net radiant heat flux from the fuel to the propellant can be derived as follows. If the fuel and propellant brightness temperatures are defined as in reference 33 so that σT_b^4 gives the correct heat flux from each region, the net heat flux to the propellant is given by

$$q_{net} = \sigma \left(T_{f_b}^4 - T_{p_b}^4\right) \tag{2-9}$$

Now, since it was assumed that the absorption coefficients were constant, the brightness temperatures can be related to the average temperatures by

$$T_f = \eta' T_{f_b} \tag{2-10}$$

and

$$T_p = \epsilon' T_{p_b} \tag{2-11}$$

where η' and ϵ' are constants.

The net heat flux is then given by

$$q_{net} = \sigma (\eta T_f^4 - \epsilon T_p^4) \tag{2.12}$$

where $\eta = (\eta')^4$ and $\epsilon = (\epsilon')^4$. The total rate of heat transfer by radiation from the fuel to the propellant is, then, given by the product of the net heat flux and the fuel surface area, or,

$$Q_{net} = \sigma A_f (\eta T_f^4 - \epsilon T_p^4) \tag{2.13}$$

The constants η and ϵ are found by calculating the heat flux from the fuel to the propellant and from the propellant to the fuel at steady state. Williams and Byrn[37] have used the Monte Carlo program CAVEAT to ascertain heat deposition in the propellant as a function of the distance from the fuel cloud surface. This information, coupled with a knowledge of the geometry of the core and the values for the absorption coefficient of hydrogen at steady state, yields values of 6.18×10^{-3} and 1.24×10^{-3} for η and ϵ, respectively (see Appendix B).

The rate of heat loss due to neutrons and gamma rays escaping from the fuel cloud is assumed to be a constant fraction x of the reactor power, and the rate of heat generation in the fuel is equal to the power. The value of x is found by dividing the space radiator power at steady state by the reactor power at steady state; the value of x is thus .0593. The reactor power is given by

$$P = \gamma' N_f \sigma_f \phi V_f \tag{2.14}$$

where γ' is a constant, N_f is the fuel atom density, σ_f is the fuel microscopic fission cross section, ϕ is the neutron flux, and V_f is the fuel volume (σ_f and ϕ are assumed to be suitably averaged over energy and space), but $\phi = nv$ where v is the average neutron velocity, so

$$P = \gamma' N_f \sigma_f \, v V_f n \tag{2-15}$$

The fuel atom density can be written

$$N_f = \frac{m_f \, A_v}{M_f \, V_f} \tag{2-16}$$

where A_v is Avogadro's number and M_f is the molecular weight of the fuel so that

$$P = \frac{\gamma' A_v \sigma_f v}{M_f} \, m_f n \tag{2-17}$$

All the parameters on the left-hand side of this equation can be assumed to be constants during small perturbations from the steady state except m_f and n. Thus, the reactor power may be written

$$P = \gamma m_f n \tag{2-18}$$

where all the constants are lumped into the single constant γ. Now, since heat loss via neutrons and gamma rays is given by $x\gamma m_f n$, the fuel heat balance may be written

$$m_f C_f \frac{dT_f}{dt} = \gamma m_f n - \sigma A_f \, (\eta T_f^4 - \epsilon T_p^4) - x\gamma m_f n \tag{2-19}$$

or,

$$\frac{dT_f}{dt} = \frac{1}{m_f C_f} \left[(1-x) \, \gamma m_f n - \sigma A_f \, (\eta T_f^4 - \epsilon T_p^4) \right] \tag{2-20}$$

An expression for the time rate of change of the propellant temperature T_p can be obtained from a similar heat balance on the propellant in the core. The rate of heat accumulation is $m_p C_p \frac{dT_p}{dt}$ where m_p and C_p are, respectively, the propellant mass and specific heat. Under the assumption that all the radiant energy emitted by the core is absorbed in the propellant, the heat source to the propellant is given by equation (2-13). The only mechanism of heat loss in this region is assumed to be the net loss of energy due to the propellant flow through the cavity; this rate is given by $\dot{m}_{p_e} h_{p_e} - \dot{m}_{p_i} h_{p_i}$ where $\dot{m}_{p_e}$ and $\dot{m}_{p_i}$ are the propellant exit and inlet mass flow rates and h_{p_e} and h_{p_i} indicate the propellant enthalpy at the cavity exit and entrance. The resulting differential equation is

$$\frac{dT_p}{dt} = \frac{1}{m_p C_p}\left[\sigma A_f \left(\eta T_f^4 - \epsilon T_p^4\right) - \left(\dot{m}_{p_e} h_{p_e} - \dot{m}_{p_i} h_{p_i}\right)\right] \tag{2-21}$$

The mass of fuel contained in the cavity must, from a mass balance, obey the relationship

$$\frac{dm_f}{dt} = \dot{m}_{f_i} - \dot{m}_{f_e} \tag{2-22}$$

$\dot{m}_{f_e}$ and $\dot{m}_{f_i}$ are, respectively, the inlet and exit fuel mass flow rates. Similarly, the mass of propellant contained in the core must be governed by

$$\frac{dm_p}{dt} = \dot{m}_{p_i} - \dot{m}_{p_e} \tag{2-23}$$

As can be seen from the conceptual drawing of the concept under study (Figure 3), the propellant must exit the cavity through a choking nozzle. The temperature and pressure of the hydrogen decrease as the gas moves through the nozzle and its thermal energy is converted to kinetic energy. These changes in propellant properties may cause a modification of the composition of the gas through recombination of the hydrogen atoms to form H_2 molecules. For the purposes of the current study, the possible change in chemical composition will be neglected, and the stagnation temperature and pressure of the propellant will be assumed to adequately describe the flow of the fluid through the nozzle. With the aforementioned assumptions, the following equation relating the mass flow rate, the temperature, and the pressure of the propellant may be written[38]

$$\dot{m} = K \frac{p}{\sqrt{T_p}} \tag{2-24}$$

K is a constant determined by the molecular constitution of the gas and the size of the choking nozzle. Since the flow of the propellant through the reactor core is restricted by the exhaust nozzle, the choked-flow equation describes the relationship between propellant flow rate and temperature and cavity pressure which must hold at each point in time. Differentiating this expression with respect to time and inserting subscripts to indicate propellant properties yields

$$\frac{d\dot{m}_{p_e}}{dt} = K\left(T_p^{-\frac{1}{2}} \frac{dp}{dt} - \frac{1}{2} T_p^{-\frac{3}{2}} p \frac{dT_p}{dt}\right) \tag{2-25}$$

The equation of state of hydrogen gives another expression, which relates the cavity pressure, the propellant temperature, and the propellant density. At lower temperatures, a suitable equation of state would be the perfect gas law, but, at the temperatures the hydrogen attains in the gaseous core reactor cavity, the H_2 molecules become dissociated and the hydrogen atoms may be ionized. R. W. Patch[36] has performed a theoretical analysis yielding thermodynamic properties of hydrogen to 100,000°K and 1000 atmospheres using the Debye-Huckel approximation for equilibrium states of the gas. A fit was made to the data of his results which indicated that the relation

$$p = R\, T_p^{1.6}\, \rho_p \tag{2-26}$$

where R is a constant and ρ_p is the hydrogen density is an accurate equation of state describing the propellant gas in the temperature range from 1000 to 100,000°R. To predict time-dependent variations, the equation of state may be differentiated to give

$$\frac{dp}{dt} = \frac{1.6p}{T_p}\frac{dT_p}{dt} + R\, T_p^{1.6}\frac{d\rho_p}{dt} \tag{2-27}$$

Parks and Lane et al.[34] have performed calculations to determine the optical constants of uranium plasmas and, from the results of this work, were able to propose an equation of state of the form

$$\rho_f = S\, p\, T_f^{-1.77} \tag{2-28}$$

where S is a constant. The above correlation agrees quite well with the results of the Parks and Lane study for pressures between 100 and 1000

atmospheres and temperatures from 20,000 to 200,000 °R which, of course, include the operating conditions of the gas-core reactor concept. Differentiating the uranium equation of state gives

$$\frac{d\rho_f}{dt} = S\left(T_f^{-1.77}\frac{dp}{dt} - 1.77\,pT_f^{-2.77}\frac{dT_f}{dt}\right) \tag{2-29}$$

which describes the variation of the fuel density with time.

Finally, a differential equation governing the fuel exit mass flow rate can be obtained from a correlation obtained by Ragsdale[6] from the work of Lanzo[31] and Johnson[32]; the correlation is expressed as

$$\left(\frac{\dot{m}_{f_e}}{\dot{m}_{p_e}}\right) = K_v\left(\frac{V_f}{V_c}\right)^3 \tag{2-30}$$

where K_v is a constant.

Solving for $\dot{m}_{f_e}$ and differentiating with respect to time results in the equation

$$\frac{d\dot{m}_{f_e}}{dt} = \left[\left(\frac{V_f}{V_c}\right)^3\frac{d\dot{m}_{p_e}}{dt} + \frac{3\dot{m}_{p_e}V_f^2}{V_c^3}\frac{dV_f}{dt}\right]K_v \tag{2-31}$$

Careful examination of the above discussion will show that equations (2-20)-(2-23), (2-25), (2-27), (2-29), and (2-31) represent a set of eight differential equations in thirteen unknowns--T_f, V_f, ρ_f, T_p, h_{p_i}, h_{p_e}, A_f, ρ_p, m_f, m_p, $\dot{m}_{p_e}$, $\dot{m}_{f_e}$, and p. V_f and ρ_p can be eliminated as follows. Since all of the fuel is assumed to be contained in a spherical cloud in which no elements other than uranium are present, V_f is simply the fuel mass divided by the fuel density, or

$$V_f = \frac{m_f}{\rho_f} \tag{2-32}$$

Of course, ρ_p may be written as the ratio of the propellant mass and the propellant volume, but the propellant volume is the cavity volume minus the fuel volume. Thus ρ_p may be written

$$\rho_p = \frac{m_p}{V_c - m_f/\rho_f} \tag{2-33}$$

Since the fuel cloud volume is also given by

$$V_f = \frac{4\pi}{3} r_f^3 , \tag{2-34}$$

the fuel cloud radius can be written as

$$r_f = \left(\frac{3m_f}{4\pi \rho_f}\right)^{\frac{1}{3}} \tag{2-35}$$

The area of the fuel cloud is given by

$$A_f = 4\pi r_f^2 \tag{2-36}$$

so that A_f becomes

$$A_f = (4\pi)^{\frac{1}{3}} \left(\frac{3m_f}{\rho_f}\right)^{\frac{2}{3}} \tag{2-37}$$

The enthalpy of the propellant at the inlet and exit of the cavity are, of course, dependent on the propellant properties at those locations. The theoretical work by Patch[36] has indicated that the enthalpy can be considered to be only a function of temperature in the range of interest of the gas-core reactor; Figure 5 is a plot of his results for a pressure of 1000 atmospheres. The dependency of the propellant enthalpy can be approximated very well by fitting six straight lines to the curve of Figure

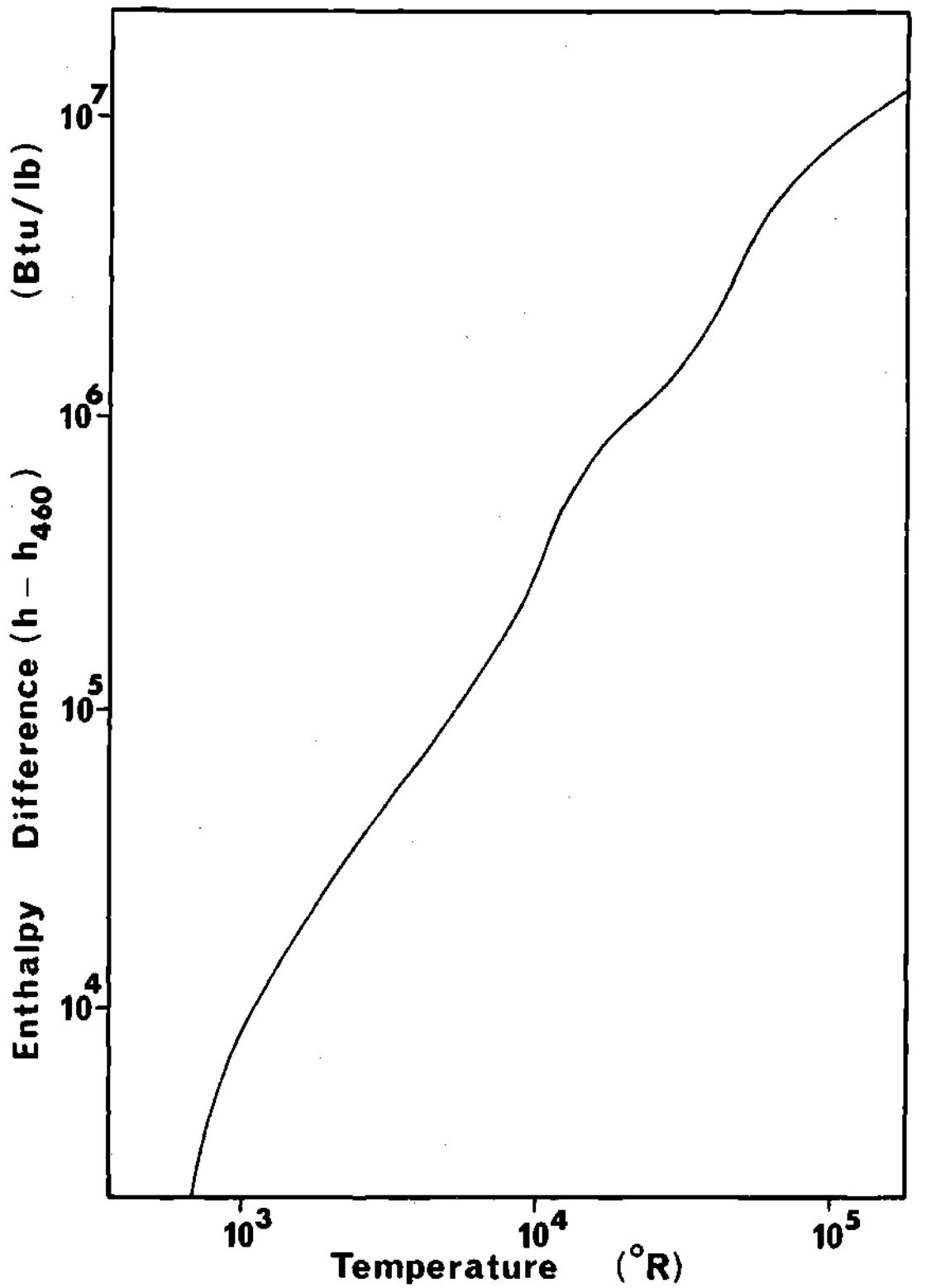

Figure 5. Hydrogen Enthalpy versus Temperature at 1000 Atmospheres

5 so that the enthalpies can be considered to be functions of the propellant temperature. The linear fit took the form of

$$\log_{10}(h) = b_i + m_i \log_{10}(T_p) \qquad (2\text{-}38)$$

where i ranged from one to six. The values for the b_i's and the m_i's and the range of temperatures for which each fit was valid are shown in Table 2.

Table 2. Constants Used in the Fit of the Hydrogen Enthalpy versus Temperature Curve of Figure 5 and Their Range of Applicability

Group	Range of Applicability (°R)	b_i	m_i
1	0 - 660	- .3648	2.514
2	660 - 4400	2.582	1.468
3	4400 - 7900	.1563	2.134
4	7900 - 18000	4.333	1.063
5	18000 - 35000	.8917	1.872
6	35000 -	6.104	.7246

Thus, the inclusion of h_{p_e} and h_{p_i} as functions of temperature removes the propellant enthalpies from the list of unknowns appearing in the cavity heat transfer and fluid dynamics equations.

As can be seen from Figure 6 (from reference 36), the hydrogen specific heat C_p is also a very strong function of the hydrogen temperature. The data of Figure 6 were also approximated by fitting six straight lines to the curve. This linear fit took the form of

$$C_p = c_i + n_i \log_{10}(T_p) \qquad (2\text{-}39)$$

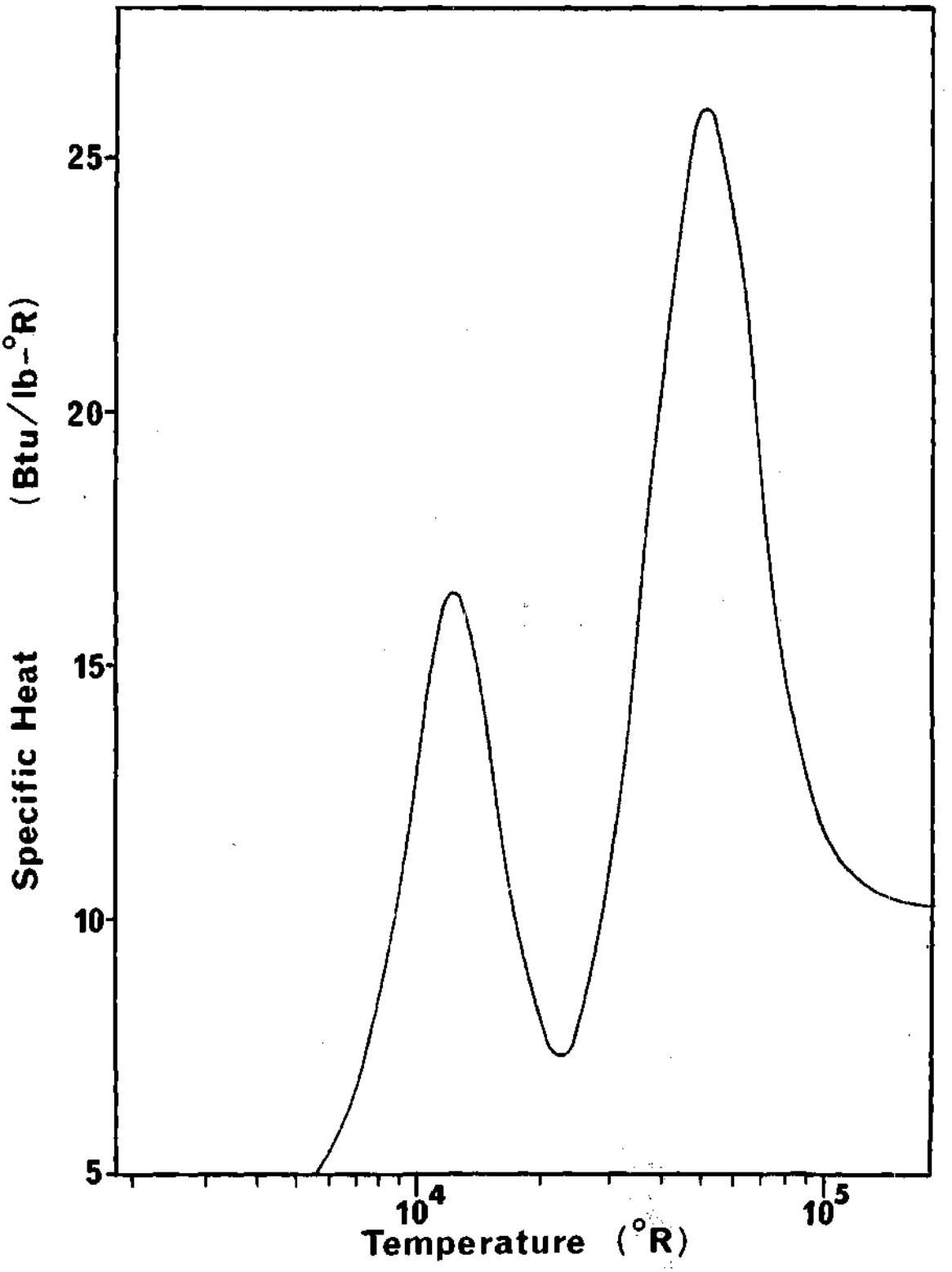

Figure 6. Hydrogen Specific Heat versus Temperature at 1000 Atmospheres

The values for the c_i's and the n_i's and the range of temperatures for which each fit was valid are shown in Table 3.

Table 3. Constants Used in the Fit of the Hydrogen Specific Heat versus Temperature Curve of Figure 6 and Their Range of Applicability

Group	Range of Applicability (°R)	c_i	n_i
1	0 - 11500	-141.97	39.0
2	11500 - 22000	156.2	34.43
3	22000 - 50000	-230.79	54.69
4	50000 - 90000	289.43	-56.02
5	90000 - 104000	146.03	-27.02
6	104000 -	40.81	6.1

Inserting the suggested expressions for V_f, A_f, and ρ_p and making use of the linear fit of the plots of propellant enthalpy and specific heat versus temperature in equations (2-20)-(2-23), (2-25), (2-27), (2-29), and (2-30) and rearranging (2-27) so that no term containing $\frac{dp}{dt}$ appears on the right-hand side (see Appendix C) yields the following group of equations which constitute a mathematical model of the dynamic behavior of the fluid flow and heat transfer processes in the reactor cavity.

$$\frac{dT_f}{dt} = \frac{1}{m_f C_f}\left[(1-x)\,\gamma \dot{m}_f n - \sigma(4\pi)^{\frac{1}{3}}\left(\frac{3m_f}{\rho_f}\right)^{\frac{2}{3}}(\eta T_f^4 - \epsilon T_p^4)\right] \qquad (2\text{-}40)$$

$$\frac{dT_p}{dt} = \frac{1}{m_p C_p}\left[\sigma(4\pi)^{\frac{1}{3}}\left(\frac{3m_f}{\rho_f}\right)^{\frac{2}{3}}(\eta T_f^4 - \epsilon T_p^4) - (\dot{m}_{p_e} h_{p_e} - \dot{m}_{p_i} h_{p_i})\right] \qquad (2\text{-}41)$$

$$\frac{dm_f}{dt} = \dot{m}_{f_i} - \dot{m}_{f_e} \qquad (2\text{-}42)$$

$$\frac{dm_p}{dt} = \dot{m}_{p_i} - \dot{m}_{p_e} \tag{2-43}$$

$$\frac{d\dot{m}_{p_e}}{dt} = K\left(T_p^{-\frac{1}{2}} \frac{dp}{dt} - \frac{1}{2} T_p^{-\frac{3}{2}} p \frac{dT_p}{dt}\right) \tag{2-44}$$

$$\frac{dp}{dt} = \frac{V_p}{V_p + V_f}\left(\frac{1.6p}{T_p}\frac{dT_p}{dt} + \frac{RT_p^{1.6}}{V_p}\frac{dm_p}{dt} + \frac{p}{V_p \rho_f}\frac{dm_f}{dt} + \frac{1.77\ V_f p}{V_f\ T_f^{1.77}}\frac{dT_f}{dt}\right) \tag{2-45}$$

$$\frac{d\rho_f}{dt} = S\left(T_f^{-1.77}\frac{dp}{dt} - 1.77\ p\ T_f^{-2.77}\frac{dT_f}{dt}\right) \tag{2-46}$$

$$\frac{d\dot{m}_{f_e}}{dt} = K_v\left[\left(\frac{V_f}{V_c}\right)^3 \frac{d\dot{m}_{p_e}}{dt} + \frac{3\dot{m}_{p_e} V_f^2}{V_c^3}\left(\frac{1}{\rho_f}\frac{dm_f}{dt} - \frac{V_f}{\rho_f}\frac{d\rho_f}{dt}\right)\right] \tag{2-47}$$

Moderator Cooling System Model

The remainder of the discussion of the equations which form the dynamics model of the coaxial flow gaseous core reactor describes the state of the moderator cooling system (Figure 4). The physical basis for each equation is a heat balance on some part of the system--the moderator itself, a heat exchanger, or a mass of coolant fluid in a component of the system. The only derivations which will be discussed in detail will be the four equations describing the operation of the primary coolant circuit; all the other relationships are derived similarly.

Denoting the moderator temperature as T_m, m_m as its mass, and C_m as its specific heat, the rate of heat accumulation in the moderator is $m_m C_m \frac{dT_m}{dt}$. The only heat source to the moderator is neutron and gamma ray heating, which, as discussed above, is given by $x\gamma m_f n$. Heat is removed

from the moderator convectively by the primary coolant which flows to the primary heat exchanger where it rejects heat to the secondary cooling circuits. The rate of heat removal from the moderator can be represented by

$$q_{rem} = h_{pc_m} A_{pc_m} (T_m - \bar{T}_{pc_m}) \tag{2-48}$$

where q_{rem} is the heat removal rate, h_{pc_m} is the appropriate heat transfer coefficient, A_{pc_m} is the moderator-to-primary-coolant heat transfer area, $\bar{T}_{pc_m}$ is the average temperature of the primary coolant in the moderator and is defined by

$$\bar{T}_{pc_m} = \frac{T_{pc_{m_e}} + T_{pc_{m_i}}}{2} \tag{2-49}$$

where the additional subscript i denotes conditions at the moderator inlet and e indicates conditions at the moderator exit. Thus, the heat balance on the moderator gives a differential equation describing the dynamic behavior of the moderator temperature as

$$\frac{dT_m}{dt} = \frac{1}{C_{m_m}} (x\gamma m_f n - h_{pc_m} A_{pc_m} (T_m - \bar{T}_{pc_m})) \tag{2-50}$$

Similarly, the rate of heat accumulation in the portion of the primary coolant inside the moderator is $m_{pc_m} C_{pc} \frac{d\bar{T}_{pc_m}}{dt}$ where m_{pc_m} is the mass of primary coolant in the moderator and C_{pc} is the specific heat of the coolant. Heat gain by the coolant in the moderator occurs at the rate at which heat is convected from the moderator, or, $h_{pc_m} A_{pc_m} (T_m - \bar{T}_{pc_m})$;

heat loss is the net rate of heat flow out of the moderator coolant passages due to coolant flow and is given by $\dot{m}_{pc} C_{pc} (T_{pc_{m_e}} - T_{pc_{m_i}})$ where $\dot{m}_{pc}$ is the primary coolant flow rate. The heat balance on the primary coolant in the moderator then gives the expression

$$\frac{d \bar{T}_{pc_m}}{dt} = \frac{1}{m_{pc_m} C_{pc}} \left\{ h_{pc_m} A_{pc_m} (T_m - \bar{T}_{pc_m}) - \dot{m}_{pc} C_{pc} (T_{pc_{m_e}} - T_{pc_{m_i}}) \right\} \quad (2\text{-}51)$$

The equation describing the heat balance on the primary coolant in the primary heat exchanger is written in the same manner as equation (2-51), except the heat gain is due to hot fluid flowing into the primary heat exchanger and the loss is by convection to the primary heat exchanger. The equation describing the behavior of the average primary coolant temperature in the primary heat exchanger thus becomes

$$\frac{d \bar{T}_{pc_{px}}}{dt} = \frac{1}{m_{pc_{px}} C_{pc}} \left\{ \dot{m}_{pc} C_{pc} (T_{pc_{px_i}} - T_{pc_{px_e}}) - h_{pc_{px}} A_{pc_{px}} (\bar{T}_{pc_{px}} - T_{px}) \right\} \quad (2\text{-}52)$$

As indicated in the derivation of equation (2-52) above, the heat source to the primary heat exchanger is the energy convectively transferred from the primary coolant. Heat is carried away from the primary heat exchanger by both the radiator and turbine coolant fluids so that the rate of heat loss may be written

$$h_{rc_{px}} A_{rc_{px}} (T_{px} - \bar{T}_{rc_{px}}) + h_{tc_{px}} A_{tc_{px}} (T_{px} - \bar{T}_{tc_{px}}) \quad (2\text{-}53)$$

The primary heat exchanger heat balance may now be written

$$\frac{d\,T_{px}}{dt} = \frac{1}{m_{px}C_{px}}\left\{h_{pc_{px}}A_{pc_{px}}\,(\bar{T}_{pc_{px}} - T_{px}) - h_{rc_{px}}A_{rc_{px}}\right. \tag{2-54}$$

$$\left. \times\,(T_{px} - \bar{T}_{rc_{px}}) - h_{tc_{px}}A_{tc_{px}}\,(T_{px} - \bar{T}_{tc_{px}})\right\}$$

which completes the derivation of the equations describing the dynamic behavior of the primary coolant loop.

Similar heat balances can be made on the remaining components of the moderator cooling system. The components and the resulting equations are:

Radiator coolant in primary heat exchanger

$$\frac{d\,\bar{T}_{rc_{px}}}{dt} = \frac{1}{m_{rc_{px}}C_{rc}}\left\{h_{rc_{px}}A_{rc_{px}}\,(T_{px} - \bar{T}_{rc_{px}})\right. \tag{2-55}$$

$$\left. - \dot{m}_{rc}C_{rc}\,(T_{rc_{px_e}} - T_{rc_{px_i}})\right\}$$

Turbine circuit fluid in primary heat exchanger

$$\frac{d\,\bar{T}_{tc_{px}}}{dt} = \frac{1}{m_{tc_{px}}C_{tc}}\left\{h_{tc_{px}}A_{tc_{px}}\,(T_{px} - \bar{T}_{tc_{px}})\right. \tag{2-56}$$

$$\left. - \dot{m}_{tc}C_{tc}\,(T_{tc_{px_e}} - T_{tc_{px_i}})\right\}$$

Radiator coolant in space radiator

$$\frac{d\,\bar{T}_{rc_r}}{dt} = \frac{1}{m_{rc_r}C_{rc}}\left\{\dot{m}_{rc}C_{rc}\,(T_{rc_{r_i}} - T_{rc_{r_e}}\right. \tag{2-57}$$

(continued)

$$- h_{rc_r} A_{rc_r} (\bar{T}_{rc_r} - T_r)\Big\}$$

Space radiator

$$\frac{d T_r}{dt} = \frac{1}{m_r C_r}\left\{h_{rc_r} A_{rc_r} (\bar{T}_{rc_r} - T_r) - \sigma A_r T_r^4\right\} \tag{2-58}$$

Turbine circuit fluid in propellant preheater

$$\frac{d \bar{T}_{tc_{pp}}}{dt} = \frac{1}{m_{tc} C_{tc}}\left\{\dot{m}_{tc} C_{tc} (T_{tc_{pp_i}} - T_{tc_{pp_e}}) - h_{tc_{pp}} A_{tc_{pp}} (\bar{T}_{tc_{pp}} - T_{pp})\right\} \tag{2-59}$$

Propellant preheater

$$\frac{d T_{pp}}{dt} = \frac{1}{m_{pp} C_{pp}}\left\{h_{tc_{pp}} A_{tc_{pp}} (\bar{T}_{tc_{pp}} - T_{pp}) - h_{p_{pp}} A_{p_{pp}} (T_{pp} - \bar{T}_{p_{pp}})\right\} \tag{2-60}$$

Propellant in propellant preheater

$$\frac{d T_{p_{pp}}}{dt} = \frac{1}{m_{p_{pp}} C_p}\left\{h_{p_{pp}} A_{p_{pp}} (T_{pp} - \bar{T}_{p_{pp}}) - \dot{m}_{p_{pp}} (h_{p_{pp_e}} - h_{p_{pp_i}})\right\} \tag{2-61}$$

The heat loss terms appearing in equations (2-58) and (2-61) are not similar to those appearing in other equations and deserve further discussion. The quantities $h_{p_{pp_e}}$ and $h_{p_{pp_i}}$ indicate the propellant enthalpy

at the exit and inlet of the propellant preheater; they can be eliminated from equation (2-61) in the same way in which h_{p_e} and h_{p_i} were removed from equation (2-21) so that $h_{p_{pp_e}}$ and $h_{p_{pp_i}}$ become functions of $T_{p_{pp_e}}$ and $T_{p_{pp_i}}$, respectively. Heat loss from the space radiator is by radiation to free space, and is given by $\sigma A_r T_r^4$, where, as discussed below, A_r is found from a knowledge of the amount of heat which must be removed from the moderator at steady state.

Equations (2-50)-(2-52) and (2-54)-(2-61) constitute 11 equations in 23 unknowns--T_m, $T_{pc_{m_i}}$, $T_{pc_{m_e}}$, $\bar{T}_{pc_m}$, $T_{pc_{px_i}}$, $T_{pc_{px_e}}$, $\bar{T}_{pc_{px}}$, T_{px}, $T_{rc_{px_i}}$, $T_{rc_{px_e}}$, $\bar{T}_{rc_{px}}$, $T_{rc_{r_i}}$, $T_{rc_{r_e}}$, $\bar{T}_{rc_r}$, T_r, $T_{tc_{px_i}}$, $\bar{T}_{tc_{px}}$, $T_{tc_{pp_i}}$, $T_{tc_{pp_e}}$, $\bar{T}_{tc_{pp}}$, T_{pp}, $T_{p_{pp_e}}$, and $\bar{T}_{p_{pp}}$, which are all functions of time ($T_{p_{pp_i}}$ is constant because the propellant is fed to the heater from a constant temperature tank). Under the assumption of no heat losses from the pipes connecting the heat exchangers and neglecting the pump work in the circuits, the relations

$$T_{pc_{m_i}}(t) = T_{pc_{px_e}}(t - \tau_{px\text{-}m}) \tag{2-62}$$

$$T_{pc_{px_i}}(t) = T_{pc_{m_e}}(t - \tau_{m\text{-}px})$$

$$T_{rc_{px_i}}(t) = T_{rc_{r_e}}(t - \tau_{r\text{-}px})$$

$$T_{rc_{r_i}}(t) = T_{rc_{px_e}}(t - \tau_{px\text{-}r})$$

$$T_{tc_{px_i}}(t) = T_{tc_{pp_e}}(t - \tau_{pp\text{-}px})$$

$$T_{tc_{pp_i}}(t) = T_{tc_{px_e}}(t - \tau_{px\text{-}pp})$$

hold where $\tau_{\alpha-\beta}$ is the time required for the fluid to flow from component α to component β; throughout this analysis, it is assumed that $\tau_{\alpha-\beta} = \tau_{\beta-\alpha}$. The definition of the average coolant temperatures for each heat exchanger ($\bar{T}_{\alpha_\beta}$ where α is the coolant and β indicates the heat exchanger) can be used to eliminate $T_{\alpha_{\beta_e}}$ from equations (2-50)-(2-52) and (2-54)-(2-61) by making the substitution

$$T_{\alpha_{\beta_e}} = 2\,\bar{T}_{\alpha_\beta} - T_{\alpha_{\beta_i}} \tag{2-63}$$

The above substitutions have the effect of reducing the number of variables appearing in the moderator cooling circuit equations to 11--T_m, T_{px}, $\bar{T}_{pc_m}$, $\bar{T}_{pc_{px}}$, $\bar{T}_{rc_{px}}$, $\bar{T}_{tc_{px}}$, $\bar{T}_{rc_r}$, $\bar{T}_{tc_{pp}}$, T_r, T_{pp}, and $\bar{T}_{p_{pp}}$.

Moderator Cooling Circuit Constants

Since the moderator cooling circuits have not been completely designed, the exact values for the heat transfer areas, heat transfer coefficients, and coolant flow rates are not known. For the purposes of this research, however, appropriate values for these constants can be obtained from a knowledge of the amount of heat each circuit must carry away at steady state. For example, the constants for the moderator end of the primary coolant loop can be derived as follows. The primary coolant circuit must convey 350 megawatts of heat during normal operation. Thus, setting $d\,\bar{T}_{pc_m}/dt = 0$ in equation (2-51) the relations

$$350\text{MW} = \dot{m}_{pc} C_{pc} \left(T_{pc_{m_e}} - T_{pc_{m_i}}\right) = h_{pc_m} A_{pc_m} \left(T_m - \bar{T}_{pc_m}\right) \tag{2-64}$$

must hold. Values for the grouped constant $(hA)_{pc_m}$ and $\dot{m}_{pc}$ can now be

found from

$$(hA)_{pc_m} = \frac{350MW}{(T_m - \bar{T}_{pc_m})} \tag{2-65}$$

and

$$\dot{m}_{pc} = \frac{350MW}{C_{pc}\,(T_{pc_{m_e}} - T_{pc_{m_i}})} \tag{2-66}$$

The remainder of the heat transfer coefficient-area groupings and coolant flow rates can be found similarly; the values are listed in Table 4.

Table 4. Moderator Cooling Circuit Heat Transfer Constants

Constant	Value
$(hA)_{pc_m}$	2655 Btu/sec-°R
$(hA)_{pc_{px}}$	2655 Btu/sec-°R
$\dot{m}_{pc}$	1145 lb/sec
$(hA)_{rc_{px}}$	2669 Btu/sec-°R
$(hA)_{tc_{px}}$	92 Btu/sec-°R
$(hA)_{rc_r}$	2464 Btu/sec-°R
$(hA)_{tc_{pp}}$	101 Btu/sec-°R
$\dot{m}_{rc}$	6511 lb/sec
$\dot{m}_{tc}$	235 lb/sec
$(hA)_{p_{pp}}$	7.45 Btu/sec-°R

Reactivity Feedback

Of course, in any reactor, changes in conditions in the reactor may result in changes in the neutronics properties characterizing the system. When modeling the time-dependent behavior of reactors, these changes in neutronics properties are taken into account by modifying the value of

ρ in equation (2-1) as the state of the reactor changes. In the case of the gas-core reactor, changes in the parameters describing the condition of the system may also imply changes in geometry and in the amount of fuel in the reactor. Studies by Robert Hyland at the NASA-Lewis Research Center and by the Idaho Nuclear Corporation have indicated that the reactivity effects of most importance for the coaxial flow gaseous core reactor system depend on the moderator temperature, fuel temperature, fuel radius, fuel mass, propellant temperature, and propellant density.

The effect on reactivity caused by a change in a system parameter can be written $\alpha_x f(\delta x)$ where α_x is a constant of proportionality called the reactivity coefficient and $f(\delta x)$ is a function of the variance of the parameter x from its steady state value x_0; $f(\delta x)$ usually takes on the form

$$\frac{x - x_0}{x_0} \tag{2-67}$$

or

$$x - x_0 \tag{2-68}$$

Writing the reactivity coefficients for the above mentioned parameters as α_{T_m}, α_{T_f}, α_{r_f}, α_{m_f}, α_{T_p}, and α_{ρ_p}, respectively, and denoting the $f(\delta x)$'s by the same subscripts, the reactivity may be written

$$\rho = \rho_i + \rho_c + \alpha_{T_m} f_{T_m} (\delta T_m) + \alpha_{T_f} f_{T_f} (\delta T_f) + \alpha_{r_f} f_{r_f} (\delta r_f) \tag{2-69}$$

$$+ \alpha_{m_f} f_{m_f} (\delta m_f) + \alpha_{T_p} f_{T_p} (\delta T_p) + \alpha_{\rho_p} f_{\rho_p} (\delta \rho_p)$$

where ρ_i is an optional arbitrarily introduced constant perturbation

reactivity and ρ_c is the reactivity introduced by a control mechanism, if any, which is triggered by changes in a system parameter. In order to use the reactivity coefficients which have been calculated for this reactor, the $f(\delta x)$'s all take on the form $(x-x_0)/x_0$ with the exception of f_{T_p} which is given by $T_p - T_{p_0}$.

Substituting the appropriate form for each function f into equation (2-69) and differentiating with respect to time yields

$$\frac{d\rho}{dt} = \frac{d\rho_c}{dt} + \frac{\alpha_{T_m}}{T_{m_0}} \frac{dT_m}{dt} + \frac{\alpha_{T_f}}{T_{f_0}} \frac{dT_f}{dt} + \frac{\alpha_{r_f}}{r_{f_0}} \frac{dr_f}{dt} + \frac{\alpha_{m_f}}{m_{f_0}} \frac{dm_f}{dt} \qquad (2\text{-}70)$$

$$+ \alpha_{T_p} \frac{dT_p}{dt} + \frac{\alpha_{\rho_p}}{\rho_{p_0}} \frac{d\rho_p}{dt}$$

Values for all the reactivity coefficients except the one associated with changes in fuel temperature have been obtained either through analytical techniques or by experiment. Table 5 is a list of the coefficients and the source for each value.

The reactivity changes due to altered fuel temperature are attributable to several different effects. Obviously, the fuel density, the fuel radius, and the fuel contained in the reactor cavity are all parameters which affect the neutronics of the reactor and which all may change when varying the fuel temperature. These effects are taken into account through the fuel mass and fuel radius coefficients of reactivity; thus, the only fuel temperature effect on reactivity is associated with the change in the neutron cross section with temperature, and α_{T_f} refers only to this type of feedback. An approximate expression for the fuel temperature coefficient of reactivity can be derived as follows.

Table 5. Reactivity Coefficients and Their Sources

Coefficient	Value	Units	Source
Moderator temperature	-.02	$\frac{\Delta k/k}{\Delta T_m/T_m}$	Critical experiments (reference 23)
Fuel radius	.24	$\frac{\Delta k/k}{\Delta r_f/r_f}$	Analysis (reference 38)
Fuel mass	.12	$\frac{\Delta k/k}{\Delta m_f/m_f}$	Critical experiments (reference 23)
Propellant temperature	$-.16 \times 10^{-5}$	$\frac{\Delta k/k}{\Delta T_p}$	Analysis (reference 38)
Propellant density	-.1	$\frac{\Delta k/k}{\Delta \rho_p/\rho_p}$	Analysis (reference 38)

The change in cross section due to change in temperature is, of course, due to an altered relative velocity between the neutrons and fuel atoms. The variance of neutron velocity with temperature is accounted for via the moderator temperature coefficient of reactivity. Thus, if the thermal neutron spectrum is assumed to be Maxwellian, the behavior of the fuel fission cross section is adequately described by

$$\frac{\sigma}{\sigma_0} \alpha \sqrt{\frac{T_{f_0}}{T_f}} \tag{2-71}$$

where σ_0 is the cross section at the reference temperature T_0. The percent change in cross section with temperature is then given by

$$\frac{\sigma - \sigma_0}{\sigma_0} \alpha \left(\sqrt{\frac{T_{f_0}}{T_f}} - 1 \right) \tag{2-72}$$

Now, since a given percent change in fission cross section has the same effect on reactivity as the same percent change in fuel mass, the reactivity effect of a change in fuel temperature is given by

$$- \alpha_{m_f} \left(\sqrt{\frac{T_{f_0}}{T_f}} - 1 \right) \tag{2-73}$$

so that the second term on the right-hand side of equation

$$- \alpha_{m_f} \frac{dT_f}{dt} \left(\frac{T_{f_0}^{\frac{1}{2}}}{2T_f^{\frac{3}{2}}} \right) \tag{2-74}$$

so that α_{T_f} is then

$$- \frac{\alpha_{m_f}}{2} \left(\frac{T_{f_0}}{T_f} \right)^{\frac{3}{2}} \qquad (2\text{-}75)$$

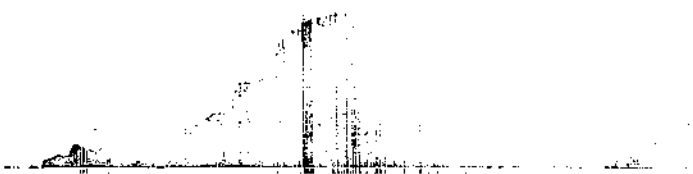

CHAPTER III

NUMERICAL METHODS

The equations developed in Chapter II (which comprise a dynamics model of the coaxial flow gaseous core reactor) can be written in the form

$$\begin{aligned} y_1' &= f_1(t, y_1, y_2, \ldots, y_n) \\ y_2' &= f_2(t, y_1, y_2, \ldots, y_n) \\ &\vdots \\ y_n' &= f_n(t, y_1, y_2, \ldots, y_n) \end{aligned} \tag{3-1}$$

where the y_i's are the neutron density, the precursor concentrations, the temperatures, etc., of Chapter II and $y_i' = \frac{dy_i}{dt}$. Equations (3-1) form a set of simultaneous first-order differential equations which, when coupled with a knowledge of the y_i's at $t = 0$, comprise what is known as an initial value problem. A group of numerical techniques called Runge-Kutta methods are often applied to solve initial value problems; the general Runge-Kutta technique can be described as follows. (This method is discussed in almost all texts on numerical methods, but the development used here parallels that presented in reference 41.)

In order to show the means of applying the Runge-Kutta method to a set of differential equations, it is convenient to describe how the method is applied to a single equation of the form

$$y' = f(t,y) \tag{3-2}$$

A Runge-Kutta method is one which employs a relation of the form

$$y^{i+1} = y^i + a_1k_1 + a_2k_2 + \ldots + a_mk_m \tag{3-3}$$

to predict the values of y over the time range of interest. The k_i's of equation (3-3) take the form

$$\begin{aligned} k_1 &= (\Delta t)f(t^i,y^i) \\ k_2 &= (\Delta t)f(t^i + p_1(\Delta t),\ y^i + q_{11}k_1) \\ &\vdots \\ k_m &= (\Delta t)f(t^i + p_{m-1}(\Delta t),\ y^i + q_{m-1,1}k_1 + \ldots + q_{m-1,m-1}k_{m-1}) \end{aligned} \tag{3-4}$$

The a's, p's, and q's must be chosen so that equation (3-3) yields correct values for the y^i's; appropriate values may be found by making equation (3-3) equivalent to a Taylor series expansion of y about t^i.

To eliminate extremely lengthy algebraic manipulations, the development of the Runge-Kutta method will be illustrated by deriving the equations for the second-order method wherein the Taylor series expansion is truncated; that is, the third and higher order terms are neglected. Expansion of y^{i+1} about t^i yields

$$y^{i+1} = y^i + (\Delta t)(y^i)' + (\Delta t)^2(y^i)'' \tag{3-5}$$

Since

$$(y^i)' = \frac{df}{dt}(t^i,y^i) \tag{3-6}$$

$(y^i)''$ is given by

$$(y^i)'' = \frac{df}{dt}(t^i,y^i) + \left[\frac{df}{dy}(t^i,y^i)\right]\left[f(t^i,y^i)\right] \tag{3-7}$$

Substituting equations (3-5) and (3-6) into equation (3-7) yields

$$y^{i+1} = y^i + (\Delta t)f(t^i,y^i) + \frac{(\Delta t)^2}{2!}\left\{\frac{df}{dt}(t^i,y^i) + \left[\frac{df}{dt}(t^i,y^i)\right]\left[f(t^i,y^i)\right]\right\} \tag{3-8}$$

An alternate expression for y^{i+1} can be obtained by expanding the expression for k_2 in the second of equations (3-4) about (t^i,y^i) and substituting the result into equation (3-3). The taylor series expansion of a function of two variables applied to this equation gives

$$k_2 = (\Delta t)\left\{f(t^i,y^i) + p_1(\Delta t)\frac{df}{dt}(t^i,y^i) + q_{11}k_1\frac{df}{dt}(t^i,y^i)\right\} \tag{3-9}$$

Substitution of the result of equation (3-9) into equation (3-3) yields (remembering that only the first three terms of equation (3-3) are being retained)

$$y^{i+1} = y^i + a_1(\Delta t)f(t^i,y^i) + a_2(\Delta t)f(t^i,y^i) \tag{3-10}$$

$$+ a_2(\Delta t)^2\left\{p_1\frac{df}{dt}(t^i,y^i) + \left[q_{11}\frac{df}{dy}(t^i,y^i)\right]\left[f(t^i,y^i)\right]\right\}$$

Equating like coefficients in equations (3-8) and (3-10) yields the three following independent equations

$$a_1 + a_2 = 1 \tag{3-11}$$

$$a_2 p_1 = \tfrac{1}{2}$$

$$a_2 q_{11} = \tfrac{1}{2}$$

Since the three equations contain four unknowns, there are an infinite number of sets of a_1, a_2, p_1, and q_{11} which satisfy the criterion of forcing equation (3-3) to yield accurate values for the y^{i+1}'s. Thus one of the four variables may be arbitrarily chosen to be unity and equation (3-11) may then be solved for the remaining unknowns.

The most popular of the Runge-Kutta methods is the fourth-order method where five terms are retained on the right-hand side of equation (3-3) and only fifth and higher order terms are neglected in the Taylor series expansions of the expressions given in equation (3-4) for k_2, k_3, and k_4. The result of carrying out a development analogous to that described above gives the following expression for y^{i+1}

$$y^{i+1} = y^i + \frac{1}{6}(k_1 + 2k_2 + 2k_3 + k_4) \tag{3-12}$$

where

$$k_1 = (\Delta t) f(t^i, y^i) \tag{3-13}$$

$$k_2 = (\Delta t) f\left(t^i + \frac{(\Delta t)}{2},\ y^i + k_1/2\right)$$

$$k_3 = (\Delta t) f(t^i + (\Delta t)/2,\ y^i + k_2/2)$$

and

$$k_4 = (\Delta t) f(t^i + (\Delta t),\ y^i + k_3)$$

The means by which the Runge-Kutta method is extended to systems of equations can be illustrated by the use of the following example.

Assume that one wishes to solve the two equation set

$$y' = f(t,y(t),u(t)) \tag{3-14}$$

$$u' = F(t,y(t),u(t))$$

by using the fourth-order Runge-Kutta integration described above. The sets of equations which would be used to get successive values of y and u would be

$$y^{i+1} = y^i + \frac{1}{6}(k_1 + 2k_2 + 2k_3 + k_4) \tag{3-15}$$

where

$$k_1 = (\Delta t)f(t^i,y^i,u^i) \tag{3-16}$$

$$k_2 = (\Delta t)f(t^i + (\Delta t)/2,\ y^i + k_1/2,\ u^i + q_1/2)$$

$$k_3 = (\Delta t)f(t^i + (\Delta t)/2,\ y^i + k_2/2,\ u^i + q_2/2)$$

$$k_4 = (\Delta t)f(t^i + (\Delta t),\ y^i + k_3,\ u^i + q_3)$$

and

$$u^{i+1} = u^i + \frac{1}{6}(q_1 + 2q_2 + 2q_3 + q_4) \tag{3-17}$$

where

$$q_1 = (\Delta t)F(t^i,y^i,u^i) \tag{3-18}$$

$$q_2 = (\Delta t)F(t^i + (\Delta t)/2,\ y^i + k_1/2,\ u^i + q_1/2)$$

$$q_3 = (\Delta t)F(t^i + (\Delta t)/2,\ y^i + k_2/2,\ u^i + q_2/2)$$

$$q_4 = (\Delta t)F(t^i + (\Delta t),\ y^i + k_3,\ u^i + q_3)$$

The method can be derived analogously for systems of more than two equations.

One extremely simple form of the Runge-Kutta method can be derived by only retaining the first term of the Taylor series expansion so that the predictor equation becomes

$$y^{i+1} = y^{i} + (\Delta t) f(t^{i}, y^{i}); \qquad (3\text{-}19)$$

when used in this form, the integration method is called Euler's method.

The choice of the method to be used in obtaining the results described in Chapter IV was limited to the fourth-order Runge-Kutta and Euler's methods. The Runge-Kutta method offers greater accuracy than Euler's for a given (Δt), but it requires a more complicated program, which, consequently, increases the program writing and development time. The choice was made as follows. The neutronics and cavity fluid flow and heat transfer equations were programmed so that either Euler's or the Runge-Kutta method could be applied. Since the moderator mass for this system is very large, transients in the moderator cooling system occur at a much slower rate than is possible in the reactor cavity. Thus, it was assumed that, if Euler's method predicted transients in the reactor cavity with comparable accuracy to the Runge-Kutta method, comparable accuracy would also be obtained for the more slowly varying moderator coolant parameters. Since the moderator coolant equations represent a large number of fairly complicated equations, a significant savings in programming time could be realized by using Euler's method for these equations. Results for the reactor cavity transients using both methods were virtually identical, so Euler's method was chosen to obtain the results described in the next chapter.

CHAPTER IV

RESULTS

The mathematical model of the coaxial flow gaseous core nuclear reactor system described in Chapter II was coupled with the numerical techniques described in Chapter III to obtain predictions of the system's response to several types of perturbations, to determine the model's sensitivity to variations in certain equations describing the dynamic processes, and to evaluate the usefulness of some possible control systems. The results which were obtained are discussed in this chapter.

The parameter of most interest insofar as reactor control is concerned is the cavity pressure, since failure to limit it to values near steady state increases significantly the likelihood of severely damaging the system. For this reason, the behavior of the cavity pressure is used as the standard of comparison in discussing these results; a pressure of 440 atmospheres (10 percent above the steady state value) is considered to be the maximum pressure allowable without incurring system damage.

Response to Perturbations in System Parameters

Reactivity Insertions

One of the perturbations of most interest in a reactor system is that of an insertion of reactivity. The predicted response of the coaxial flow reactor to a step insertion of .1 percent reactivity is shown in Figure 7.

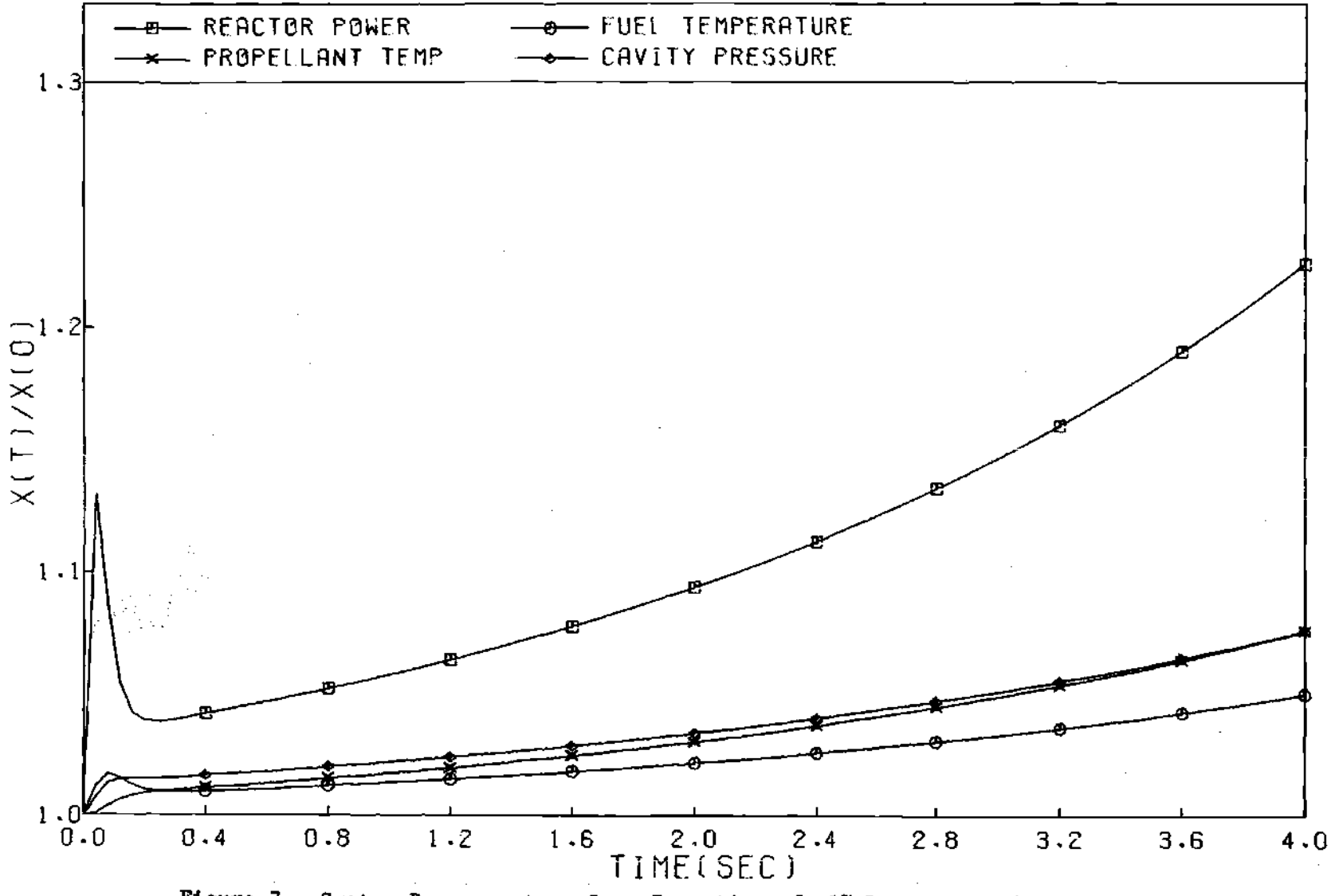

Figure 7. System Response to a Step Insertion of .1% Reactivity (to 4.0 seconds)

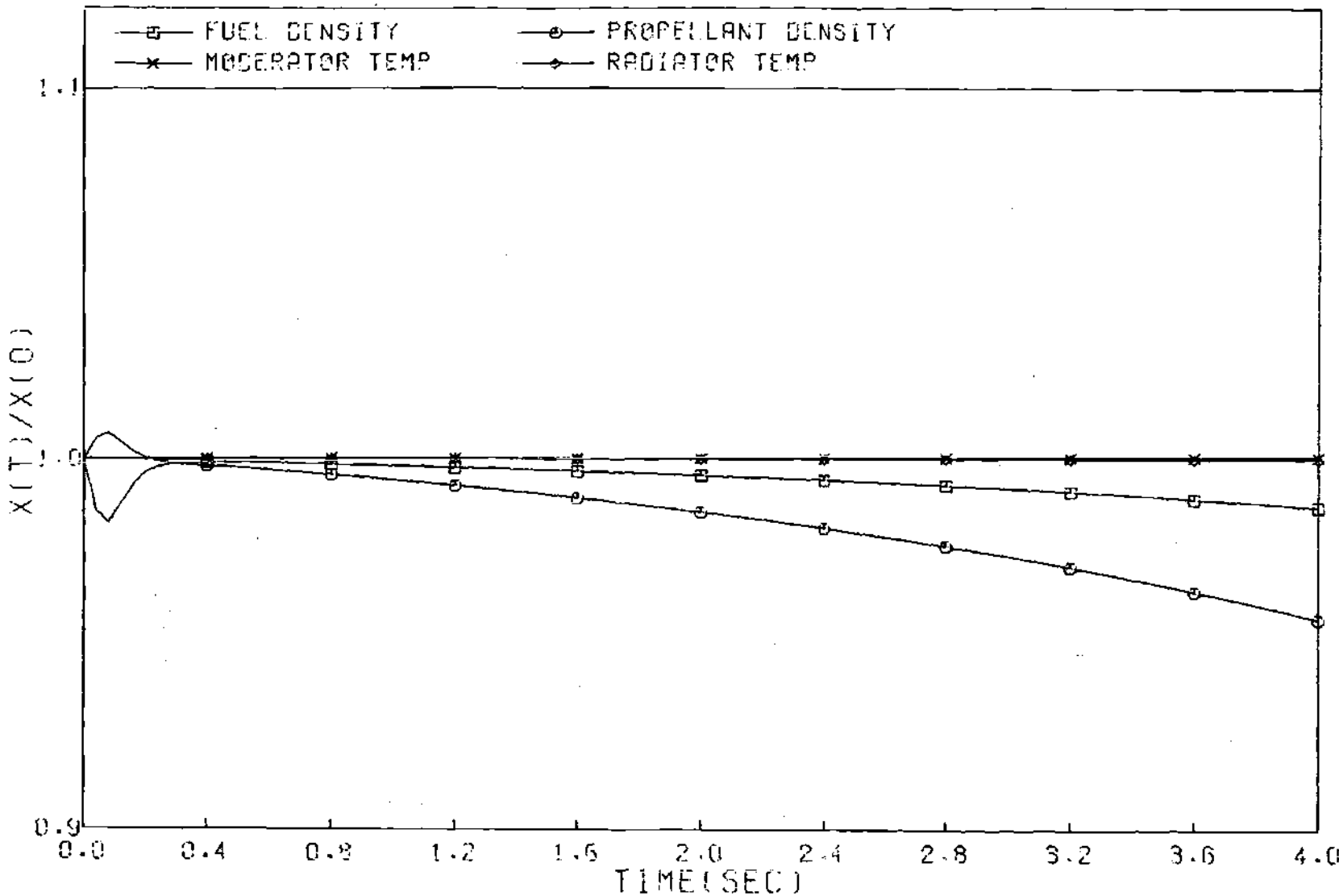

Figure 7. Continued

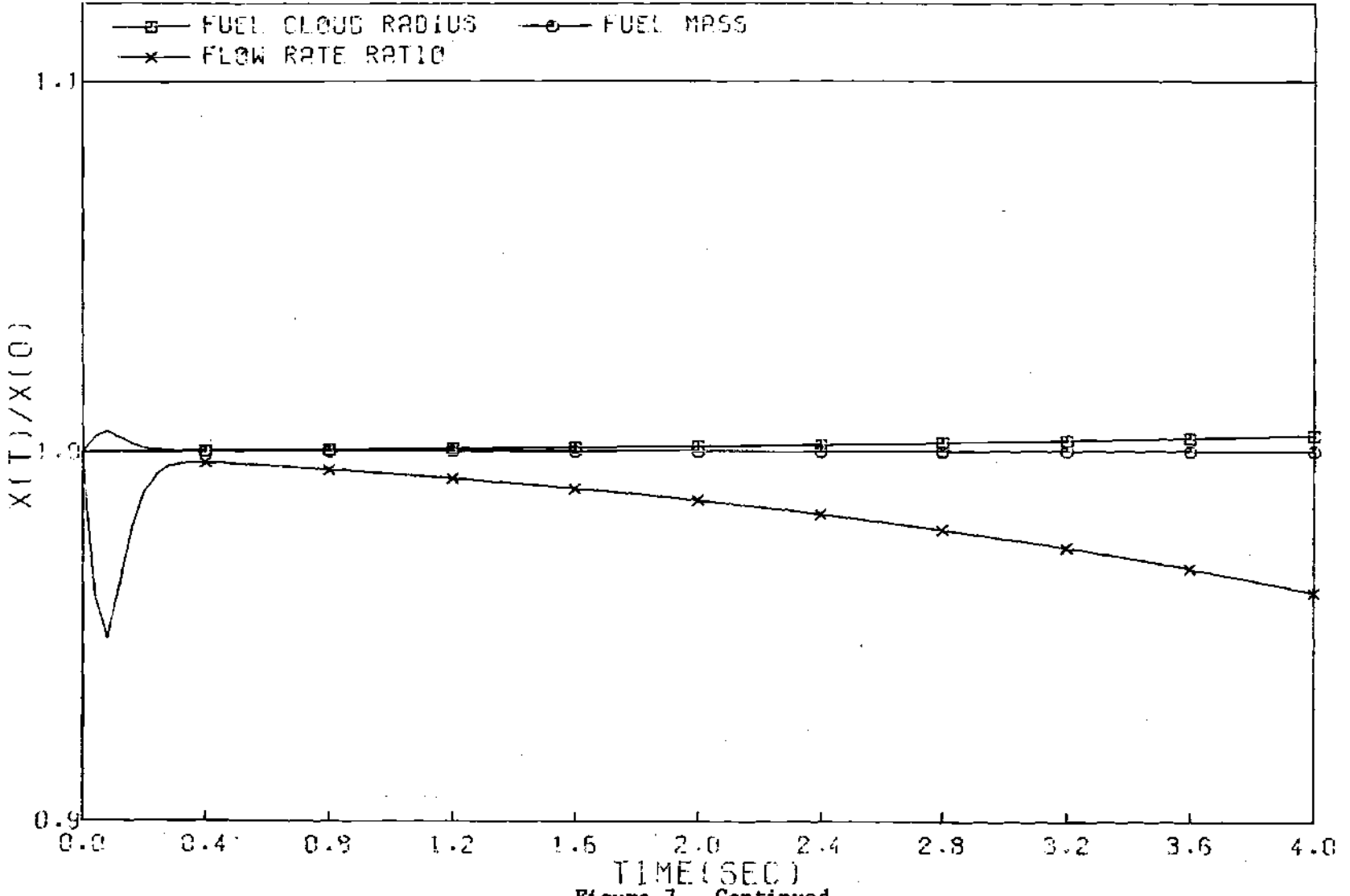

Figure 7. Continued

The response is characterized by a sharp rise in reactor power immediately after the reactivity insertion followed by an equally sharp falloff in power a short time later. After this initial peak, the power, the cavity pressure, and the fuel and propellant temperatures begin an increasingly rapid rise over the remainder of the period of the calculation. Both the fuel and the propellant density drop slightly as a result of the perturbation as does the mass exit flow rate ratio ($\dot{m}_{p_e}/\dot{m}_{f_e}$). The fuel mass, the fuel cloud radius, and the moderator and radiator temperatures do not change appreciably.

As can be seen from Figure 7, the cavity pressure does not reach 110 percent of its steady state value before four seconds after the reactivity insertion; this time is considerably longer than the response time of current control systems, so limitation of the cavity pressure following this type of perturbation should be possible.

The behavior of the reactor power immediately following the insertion can be better understood by examining the expanded plot of Figure 8 and the reactivity feedback plots of Figure 9. The power rises initially due to the increase in reactivity, but rapid increases in propellant density and fuel temperature generate sufficient negative feedback reactivity to decrease the total reactivity of the system which, in turn, causes a drop in power level. Expansion of the fuel cloud immediately after the perturbation contributes some positive reactivity feedback, but this effect is overshadowed by the negative propellant density and fuel temperature effects. Additional negative feedback is provided through the increase in propellant temperature, but it does not occur on a short enough

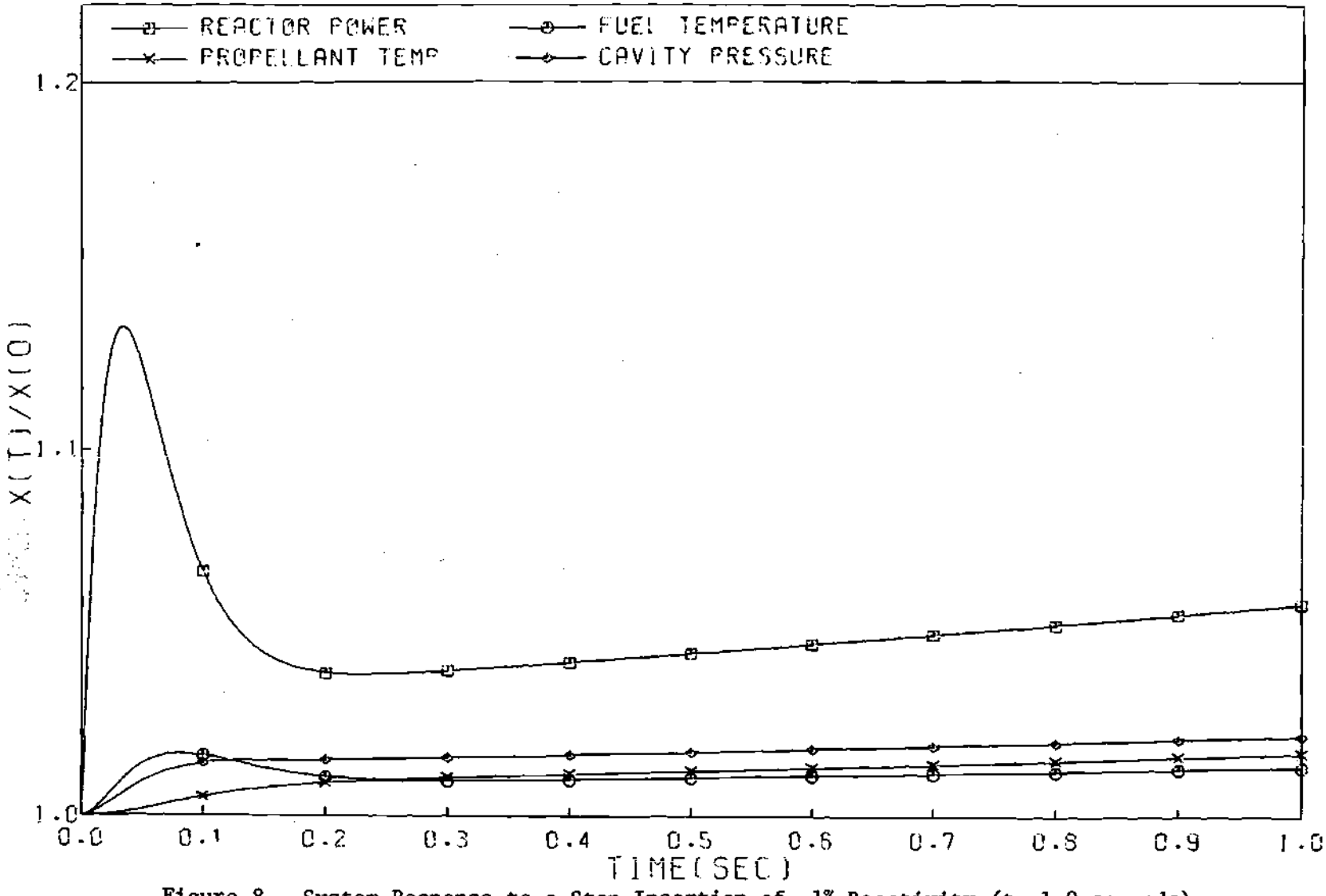

Figure 8. System Response to a Step Insertion of .1% Reactivity (to 1.0 seconds)

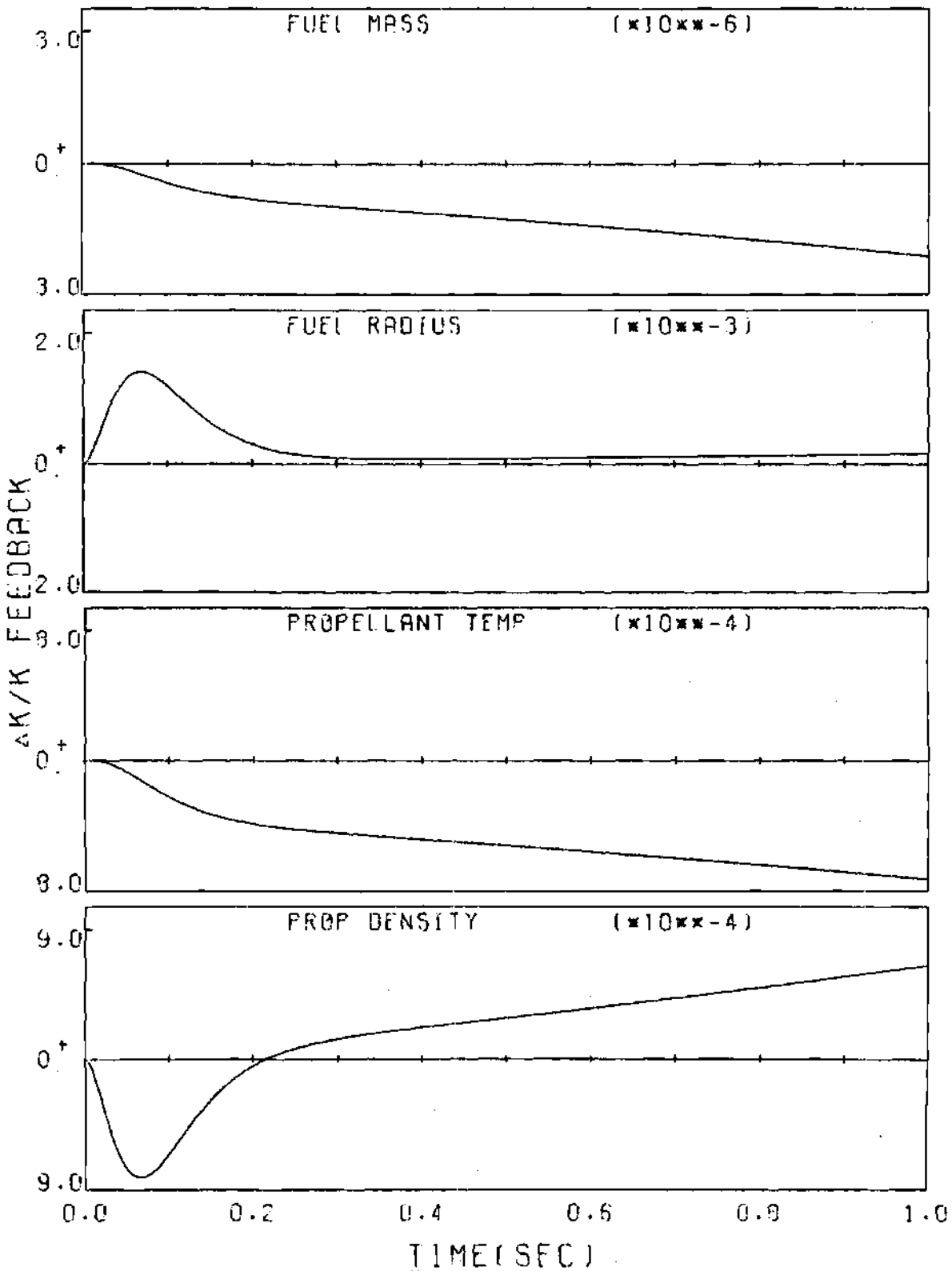

Figure 9. Components of Feedback Reactivity Following a Step Insertion of .1% Reactivity (to 1.0 seconds)

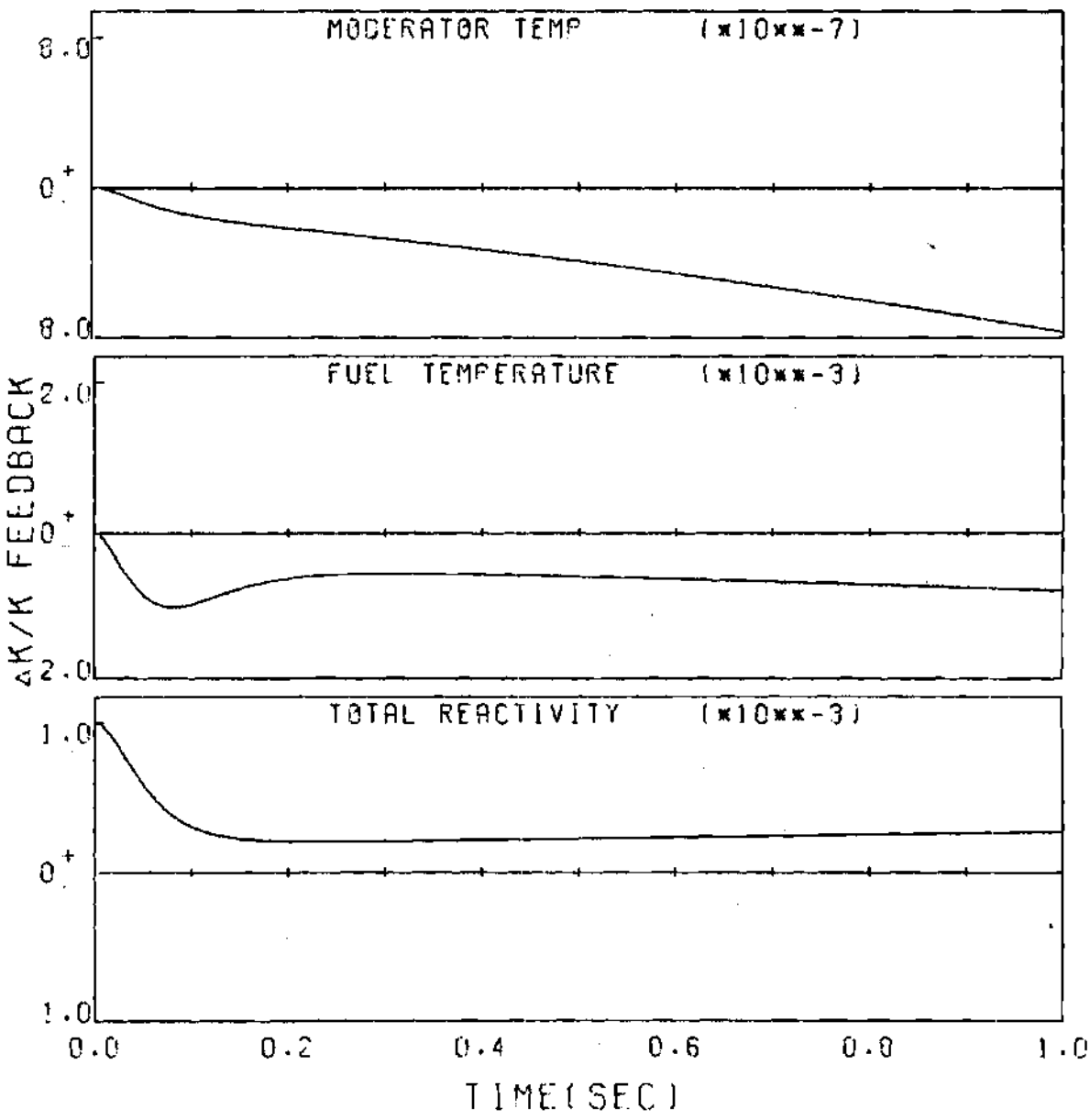

Figure 9. Continued

time scale to be a significant factor in the early power drop. Approximately 200 milliseconds after the reactivity insertion, the propellant density feedback component becomes positive and begins a steady rise in value. The transition from the sharp decrease in power to the slow rise after 200 milliseconds is thus due primarily to the change in sign of the propellant density feedback reactivity. The slower power rise at later times is a result of the positive fuel cloud radius and propellant density contributions increasing slightly faster than the negative fuel and propellant temperature feedback reactivities. Neither the fuel mass nor the moderator temperature feedback reactivities are significant in determining the time behavior of the reactor because neither parameter varies noticeably from its steady state value.

The system response to larger reactivity insertions is qualitatively the same as that shown in Figures 7 and 8. The early power peak occurs at a shorter time following the reactivity insertion and has a higher maximum value for larger perturbations. The cavity pressure also increases more sharply during the first 1000 milliseconds for larger insertions. For a step insertion of one dollar (.645 percent) of reactivity, the peak power occurred at 33 milliseconds; the cavity pressure increased to 440 atmospheres by 53 milliseconds after the perturbation. The introduction of large amounts of reactivity thus presents a much more serious control problem.

Response to Changes in Flow Rates

The system's response was predicted for the case of a 10 percent loss and a 10 percent increase in propellant inlet mass flow rate, a total

shutoff of fuel input to the cavity, and a total loss of primary coolant flow. These predictions were obtained both to indicate if dangerous conditions developed and to evaluate regulation of these flow rates as a possible control mechanism.

The predicted system response for a 10 percent loss of propellant flow at the cavity inlet is shown in Figure 10. The response is obviously a rapid increase in reactor power and, more importantly, cavity pressure; the cavity pressure reaches 110 percent of its steady state value shortly after one second following the perturbation. The attainment of the "critical" pressure occurs considerably sooner than predicted following the .1 percent reactivity insertion, but the time scale is still somewhat longer than the response time of current reactor controls. Again, the mechanism by which the response is produced can be found by examining the feedback reactivity plots of Figure 11. The initial power rise is caused by an increase in the fuel cloud radius resulting in a positive reactivity insertion whose magnitude increases with time. This positive reactivity is enhanced at later times by a positive propellant density contribution. The positive fuel radius and propellant density contributions more than cancel the negative feedback reactivity contributions from the fuel and propellant temperature increases. Again, the fuel and moderator temperature feedback effects are not major determiners of reactor behavior. Obviously, the loss of all or part of the propellant flow at the reactor cavity entrance provides a significant if not serious control problem.

Not surprisingly, the predicted response to a 10 percent increase in propellant inlet flow, as shown in Figure 12, is a reactor shutdown.

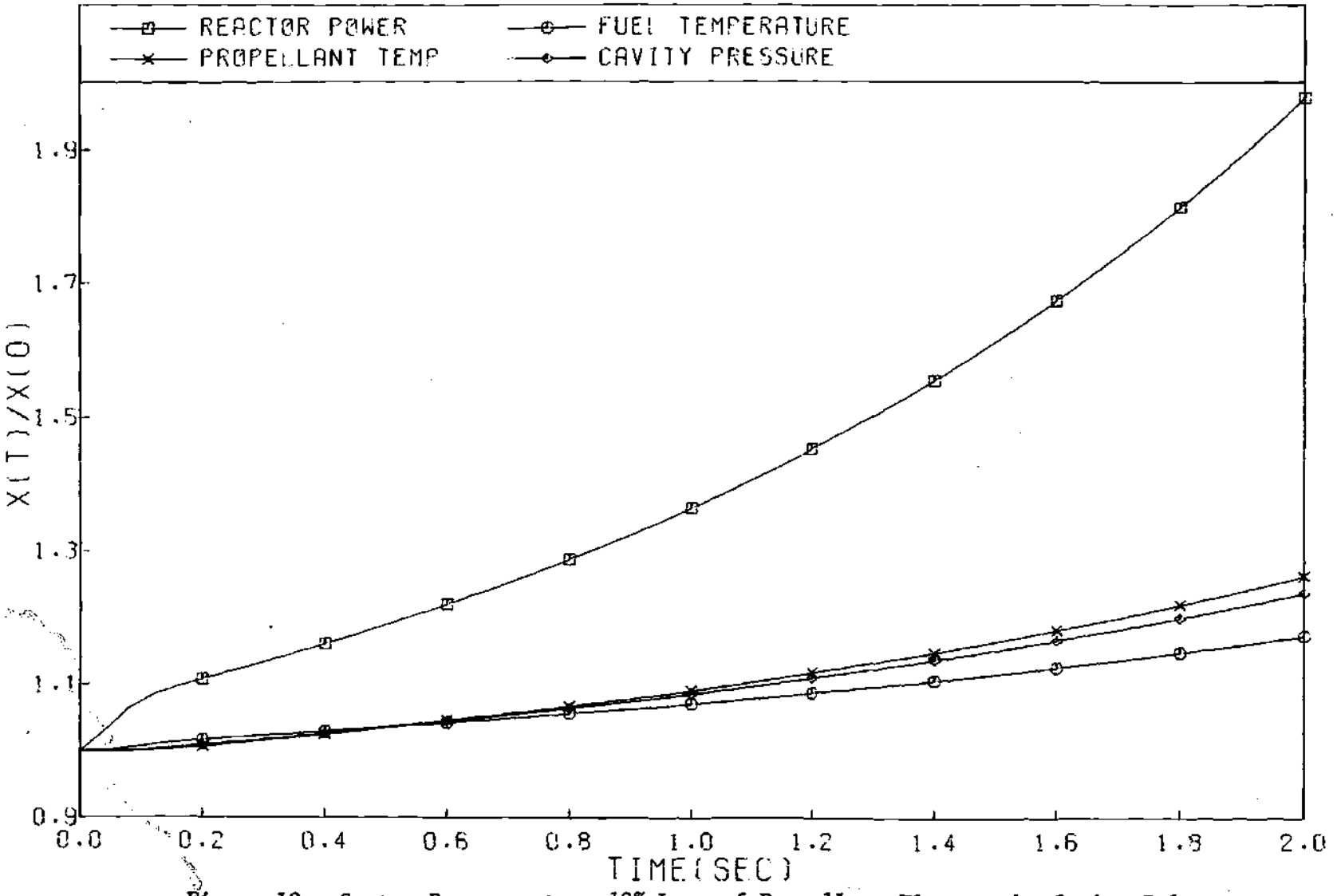

Figure 10. System Response to a 10% Loss of Propellant Flow at the Cavity Inlet

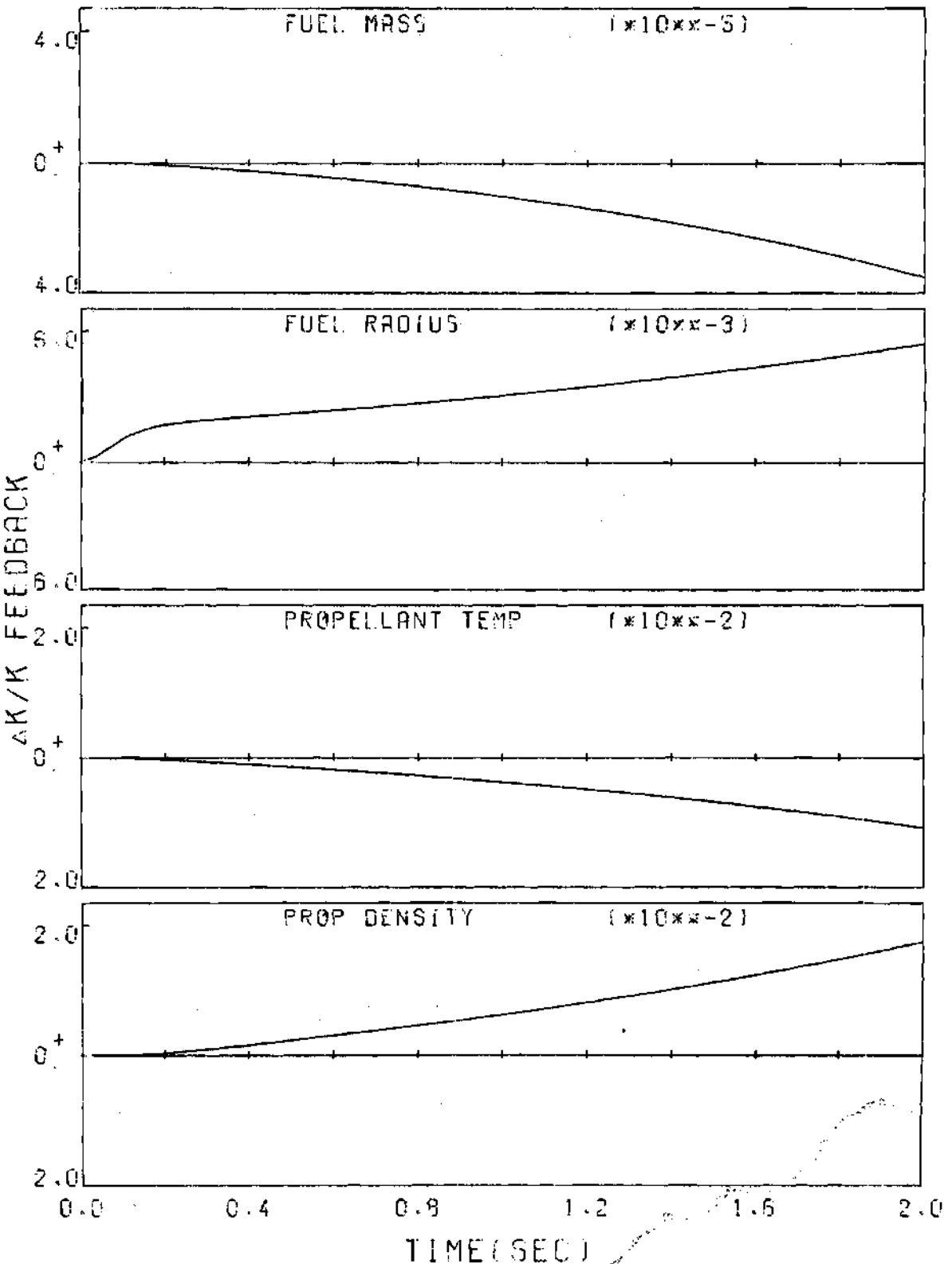

Figure 11. Components of Feedback Reactivity Following a 10% Loss of Propellant Flow at the Cavity Inlet

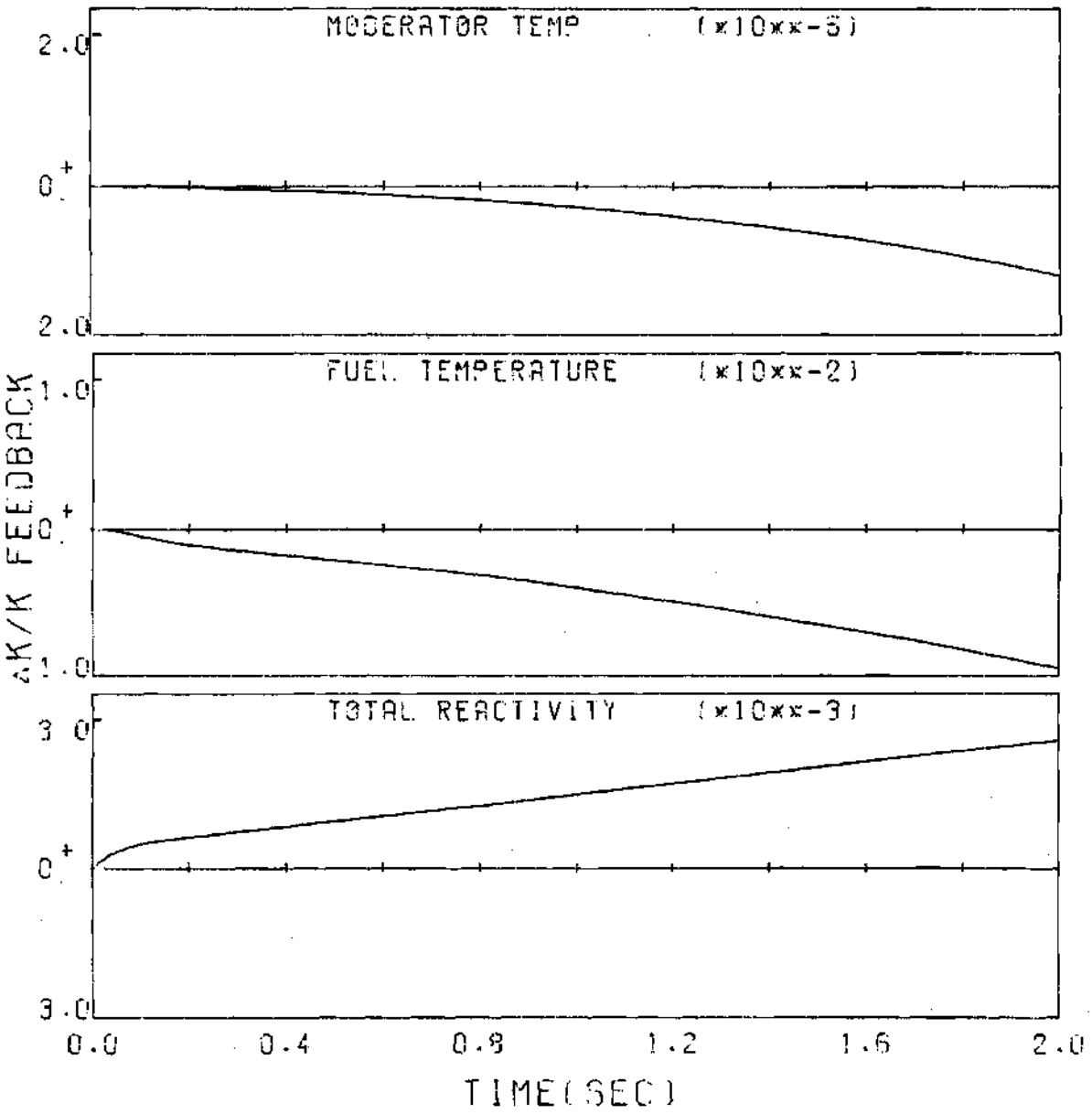

Figure 11. Continued

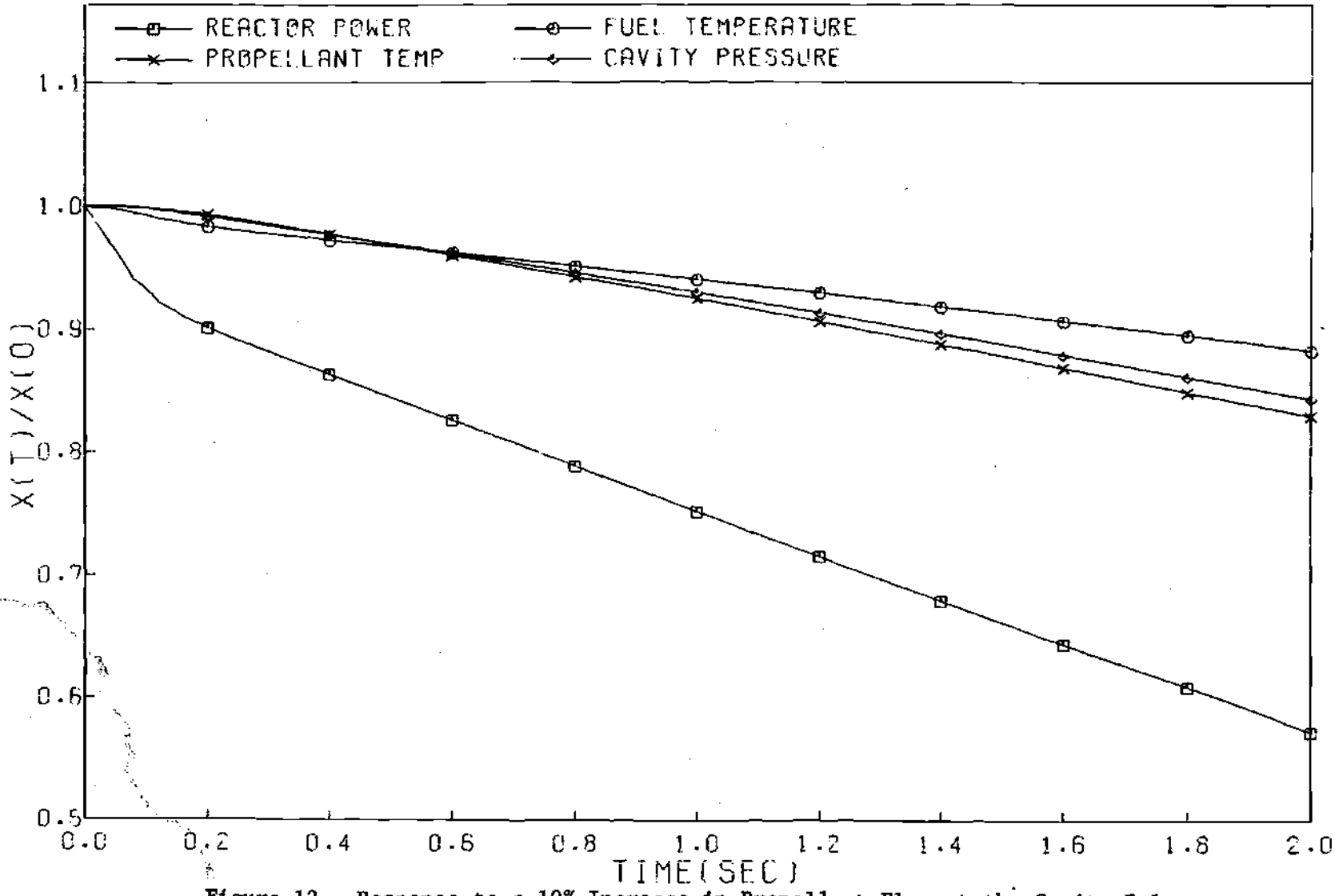

Figure 12. Response to a 10% Increase in Propellant Flow at the Cavity Inlet

All reactivity effects (shown in Figure 13) are opposite in sign to those produced in the loss of propellant flow perturbation, but the rate of negative reactivity insertion after about 0.8 seconds is slightly faster than the rate of positive insertion predicted in Figure 11.

As shown in Figure 14, the response to a complete shut-off of fuel input to the reactor cavity is also a system shutdown. The fuel loss rate is not significantly affected by this perturbation, so fuel is lost from the core; the net reduction in fuel mass causes the reactor to go subcritical, and the continued fuel loss increases the degree of subcriticality. Since the fuel residence time is rather long, the fuel is not lost very rapidly, and, consequently, the power response is not as fast as in the responses discussed above.

Figure 15 is a plot of the moderator temperature and the reactor power following a 100 percent loss in primary coolant flow. As expected, the moderator temperature rises, which causes a drop in power due to the negative moderator temperature reactivity coefficient. The slow moderator temperature rise is due to the large moderator mass and due to the increasingly rapid drop in power level. Obviously, the moderator temperature cannot decrease as long as the heat removal from it is zero, but, since it has reached a value only 36 degrees higher than the nominal operating temperature after 10 seconds, the power falloff provides a fairly long time in which emergency cooling can be provided without incurring moderator damage.

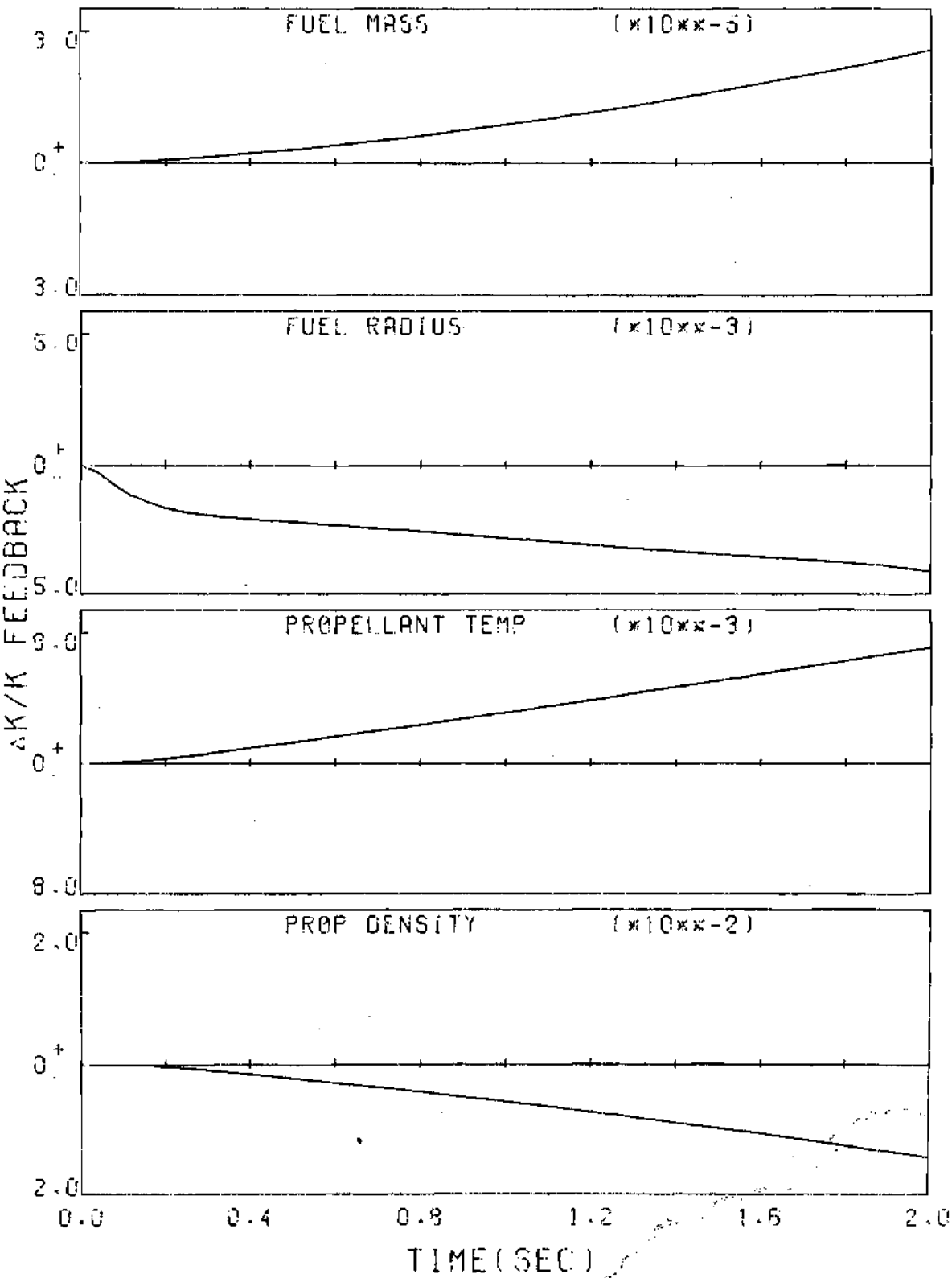

Figure 13. Components of Feedback Reactivity Following a 10% Increase in Propellant Flow at the Cavity Inlet

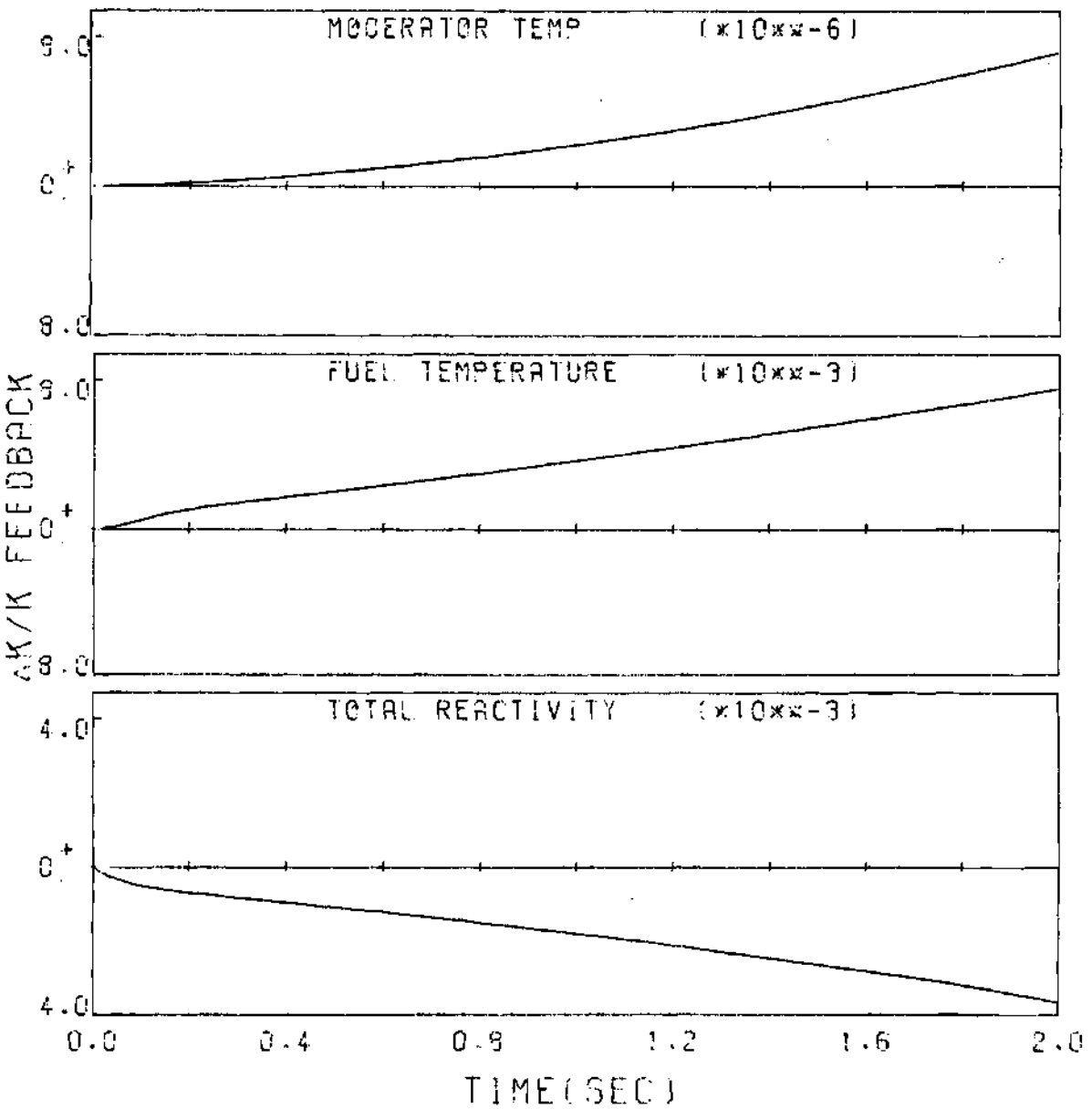

Figure 13. Continued

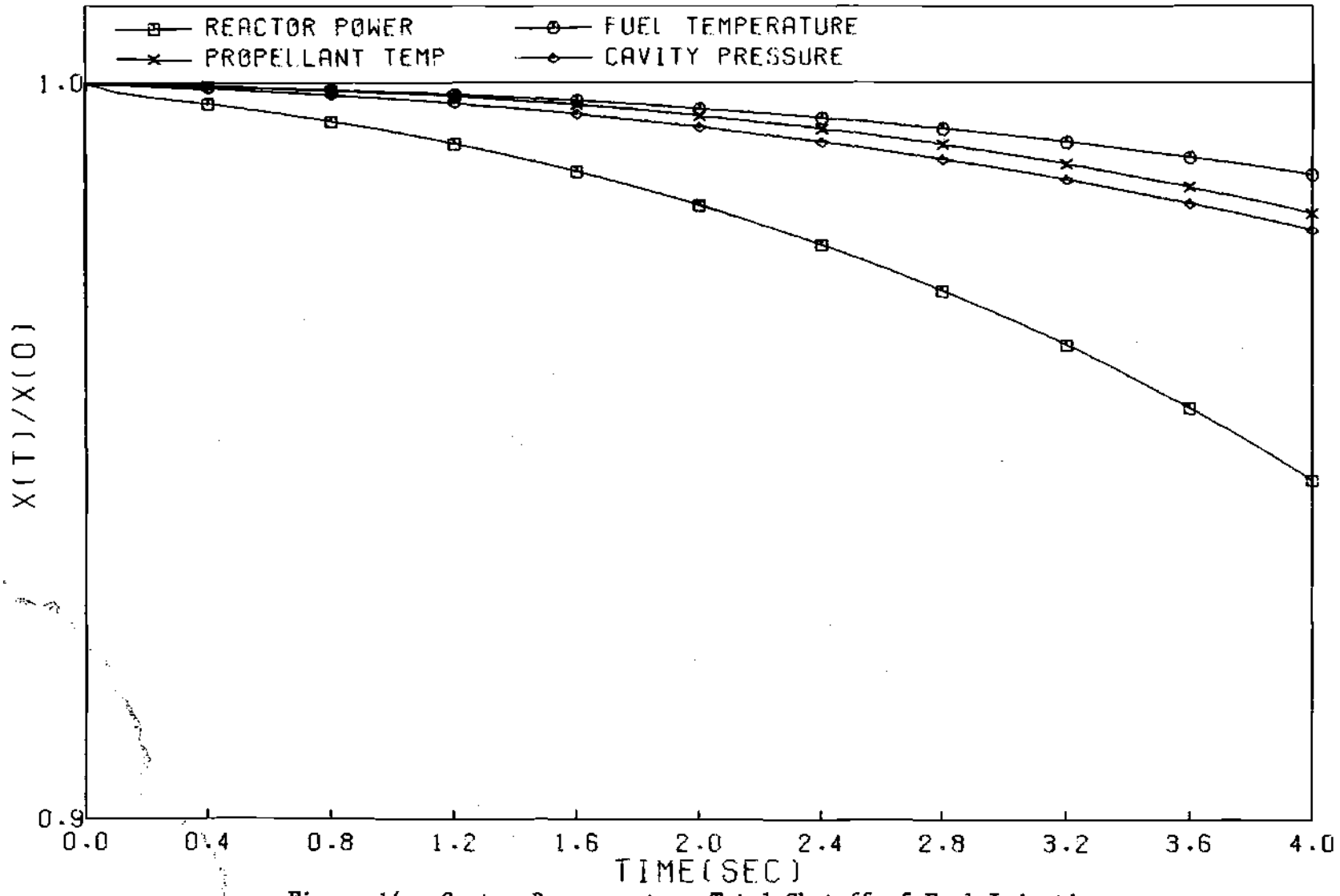

Figure 14. System Response to a Total Shutoff of Fuel Injection

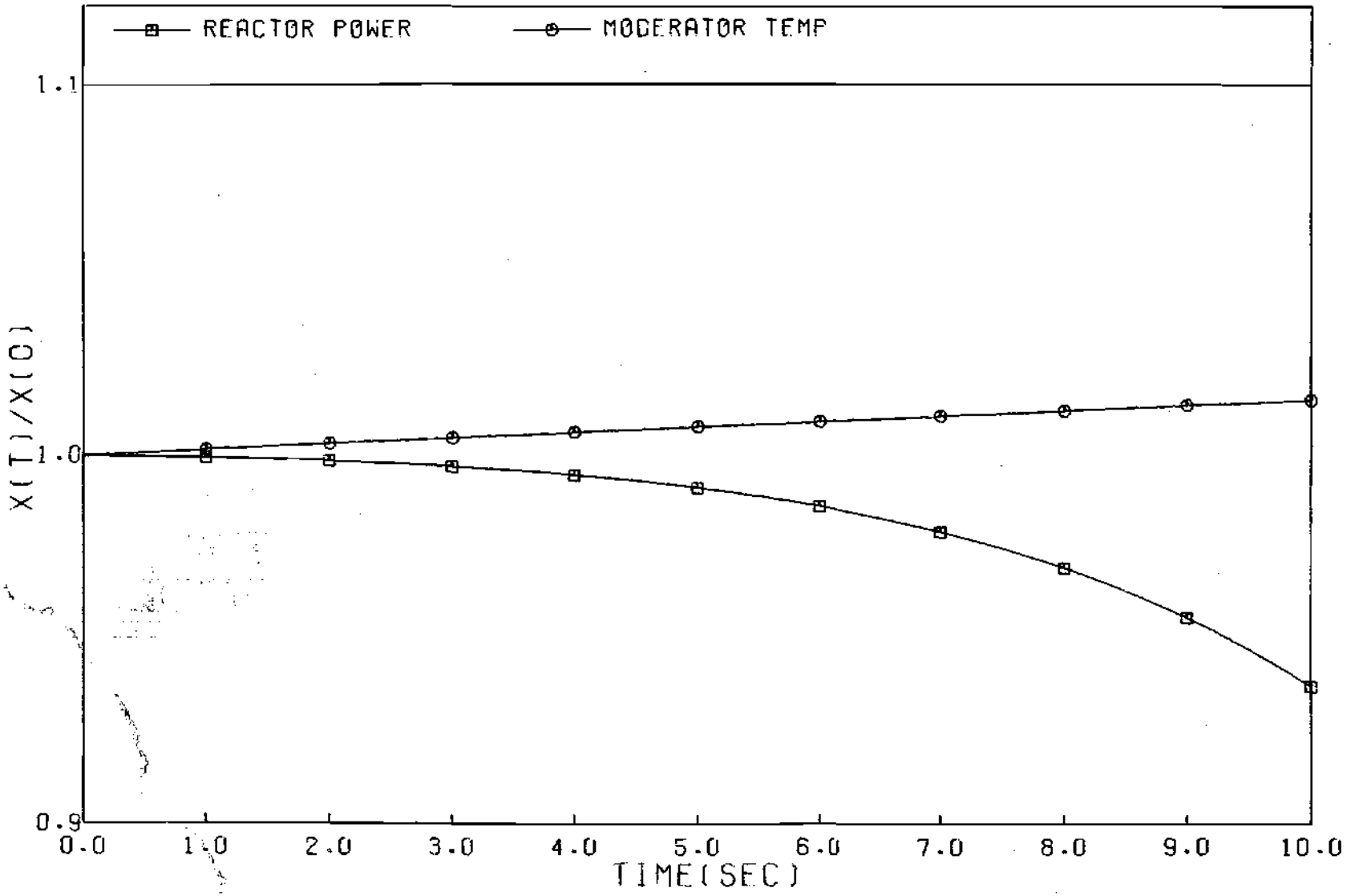

Figure 15. System Response to a 100% Loss of Moderator Primary Coolant

Determination of the Model's Sensitivity to Equation Variations

The sensitivity of the model to variations in the six reactivity coefficients was evaluated by making six additional predictions of the system response to a .1 percent reactivity insertion with one of the reactivity coefficients increased by 50 percent over the nominal value in each run. The results were then compared to the response predicted in Figure 7. A similar technique was used to find the effect on the model of changing the exponent of equation (2-30) (which described the behavior of the fuel exit mass flow rate) from three to two.

The responses utilizing increased fuel mass and moderator temperature reactivity coefficients were virtually identical to the results shown in Figure 7. This result is not surprising since neither the fuel mass nor the moderator temperature change significantly following the perturbation.

The response of the model using an increase in the propellant temperature coefficient--shown in Figure 16--is slightly more sluggish than the response of the standard model. The reactor power increases about 23 percent in four seconds using the standard model whereas the power increases 11 percent in the same time when the larger α_{T_p} is used; rises in cavity pressure, fuel temperature, and propellant temperature are correspondingly smaller in the latter case. Since the propellant temperature rises in both cases, the reason for the more sluggish response with the larger α_{T_p} is simply that the negative reactivity contribution due to propellant temperature rise is proportionally larger.

Increasing the fuel temperature coefficient of reactivity has almost

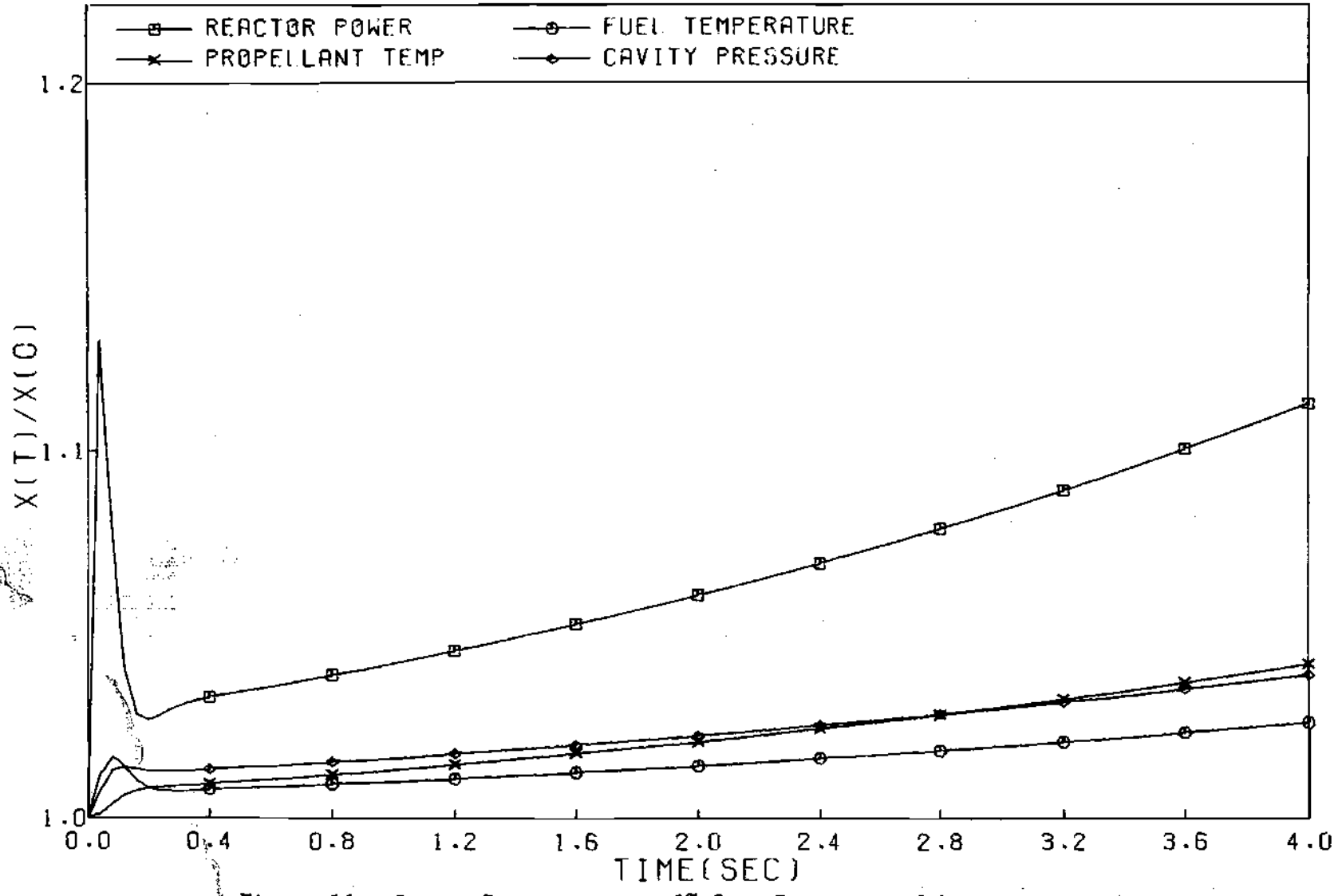

Figure 16. System Response to a .1% Step Insertion of Reactivity with α_{T_p} Increased by 50%

exactly the same effect as increasing the propellant temperature coefficient, and, again, the reason is simply that the negative contribution due to increasing fuel temperature is larger with a larger α_{T_f}.

As can be seen from Figure 17, an increase in the propellant density coefficient of reactivity has a relatively drastic effect on the system's response. The reactor power increases about 75 percent over a four second period compared to the 23 percent increase of Figure 7. Perhaps more importantly, the cavity pressure increases to 110 percent of the steady state value about three seconds after the reactivity insertion; this is, of course, a shorter time for attainment of the critical pressure than predicted by the standard model. Since the propellant density decreases during power level increases, the added rapidity of response is due to a larger positive reactivity contribution due to the larger negative reactivity coefficient.

The response for a .1 percent reactivity insertion with a larger fuel cloud radius coefficient is depicted in Figure 18. Obviously, the response is considerably different from any of those discussed above. Some insight into the processes taking place can be gotten from the reactivity plots of Figure 19. The additional positive feedback reactivity from the fuel cloud expansion accompanying the initial power rise causes the power to reach a higher value before the changes in parameters producing negative feedback (propellant density, fuel temperature, and propellant temperature) become large enough to cause a decrease in power level. The result is that so much negative feedback is inserted that the parameters governing the feedback reactivity reverse their initial behavior

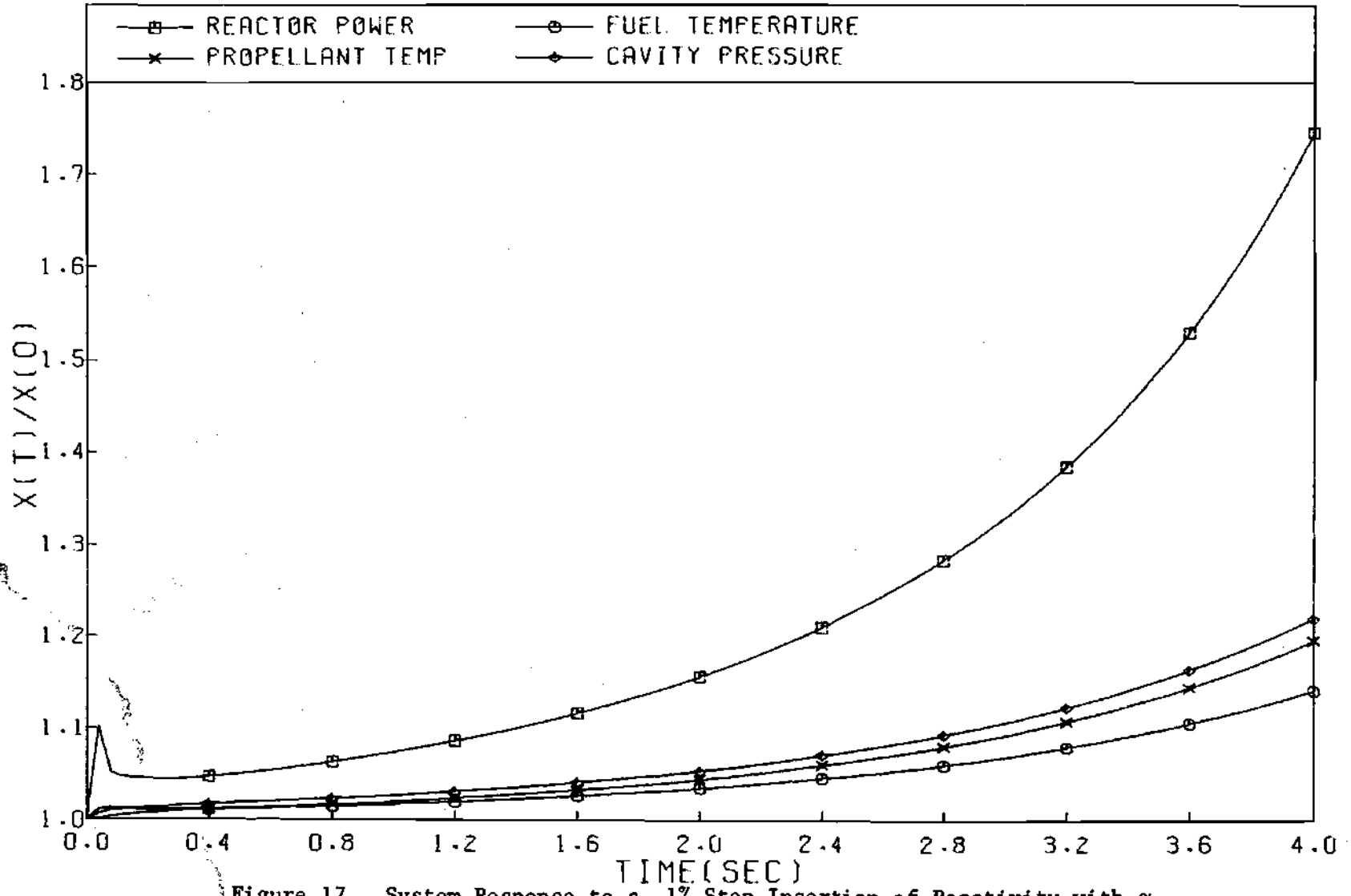

Figure 17. System Response to a .1% Step Insertion of Reactivity with α_{ρ_p} Increased by 50%

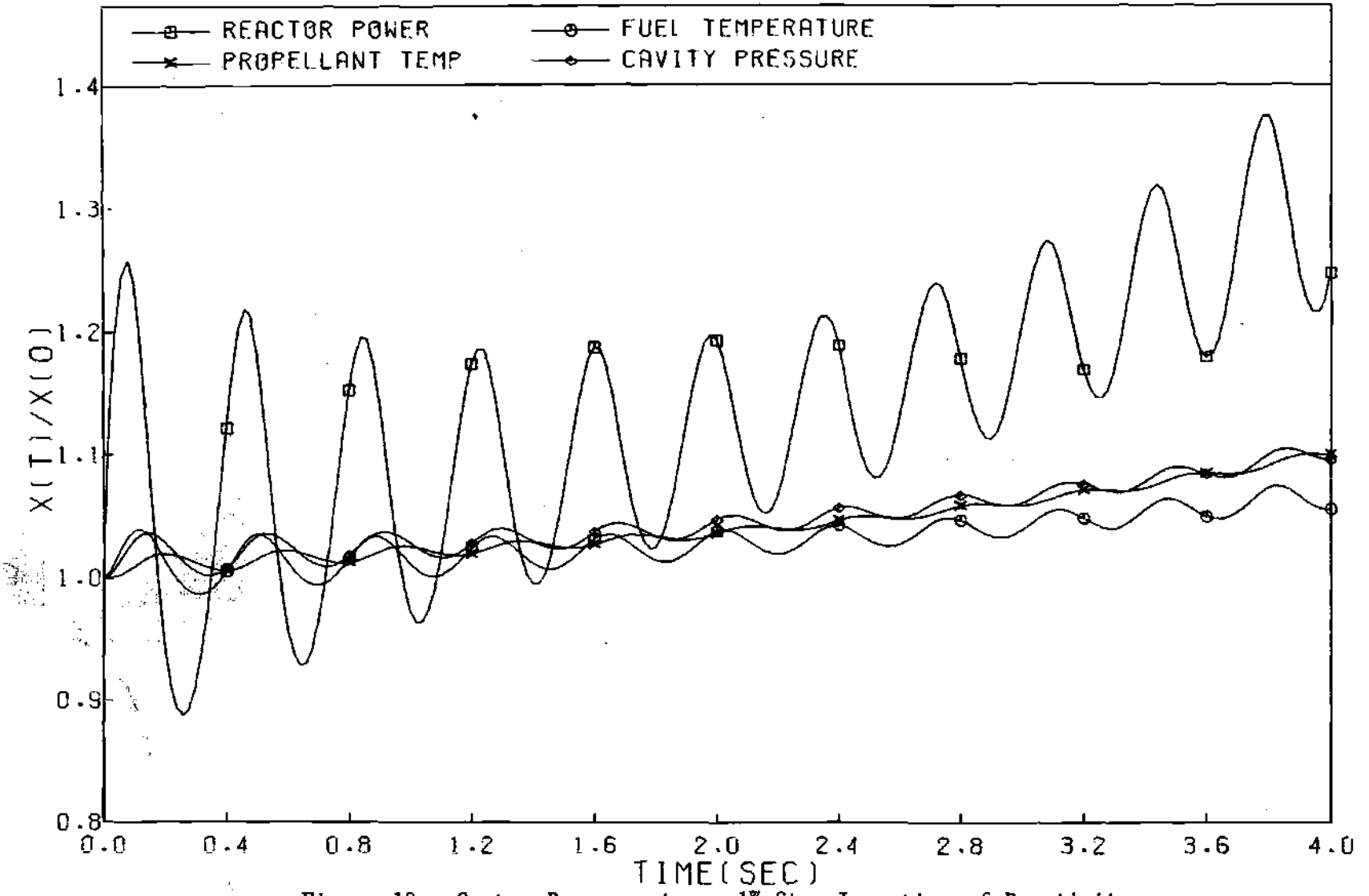

Figure 18. System Response to a .1% Step Insertion of Reactivity with α_{r_f} Increased by 50%

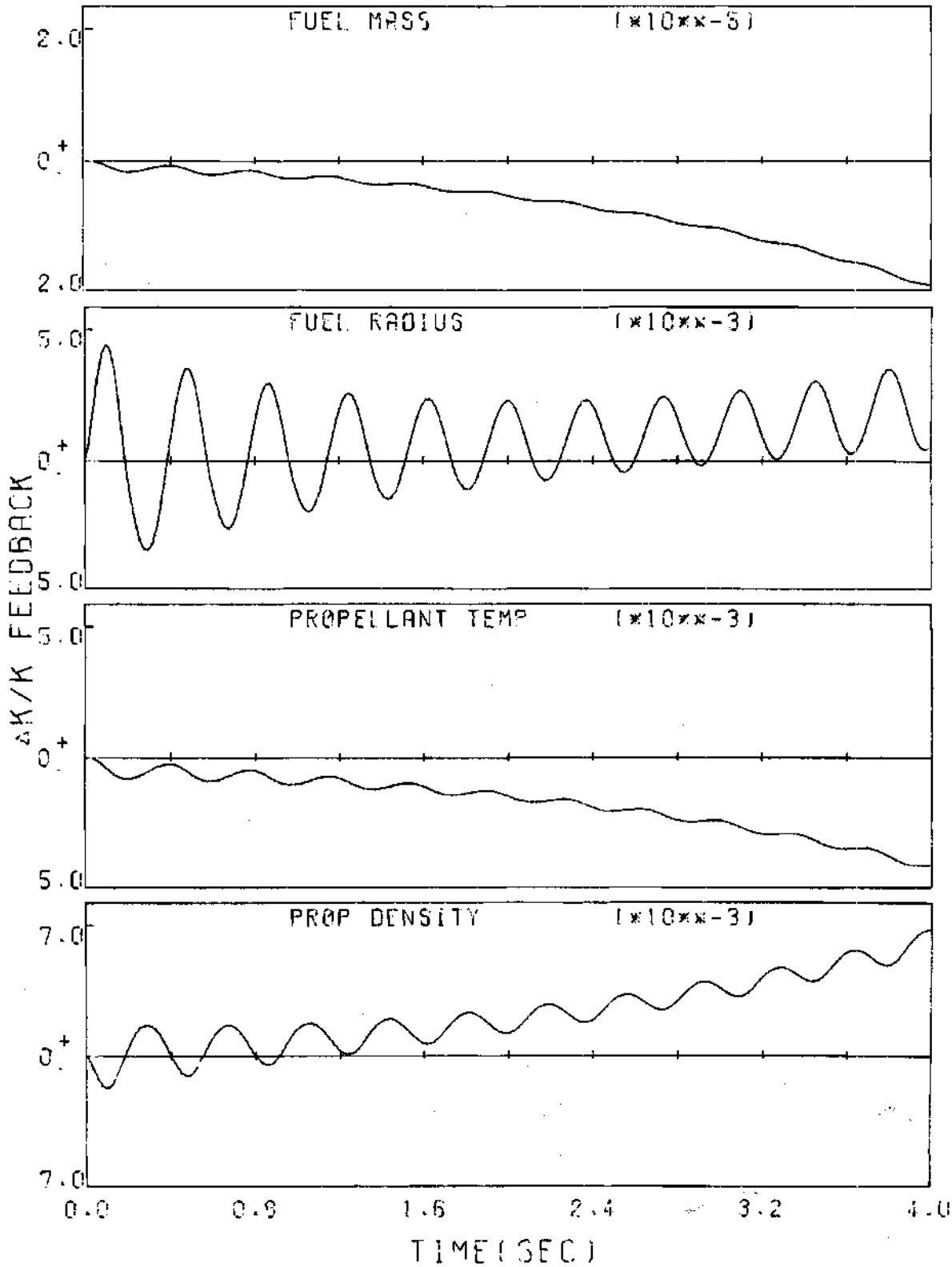

Figure 19. Components of Feedback Reactivity Following a Step Insertion of .1% Reactivity with a 50% Increase in α_{r_f}

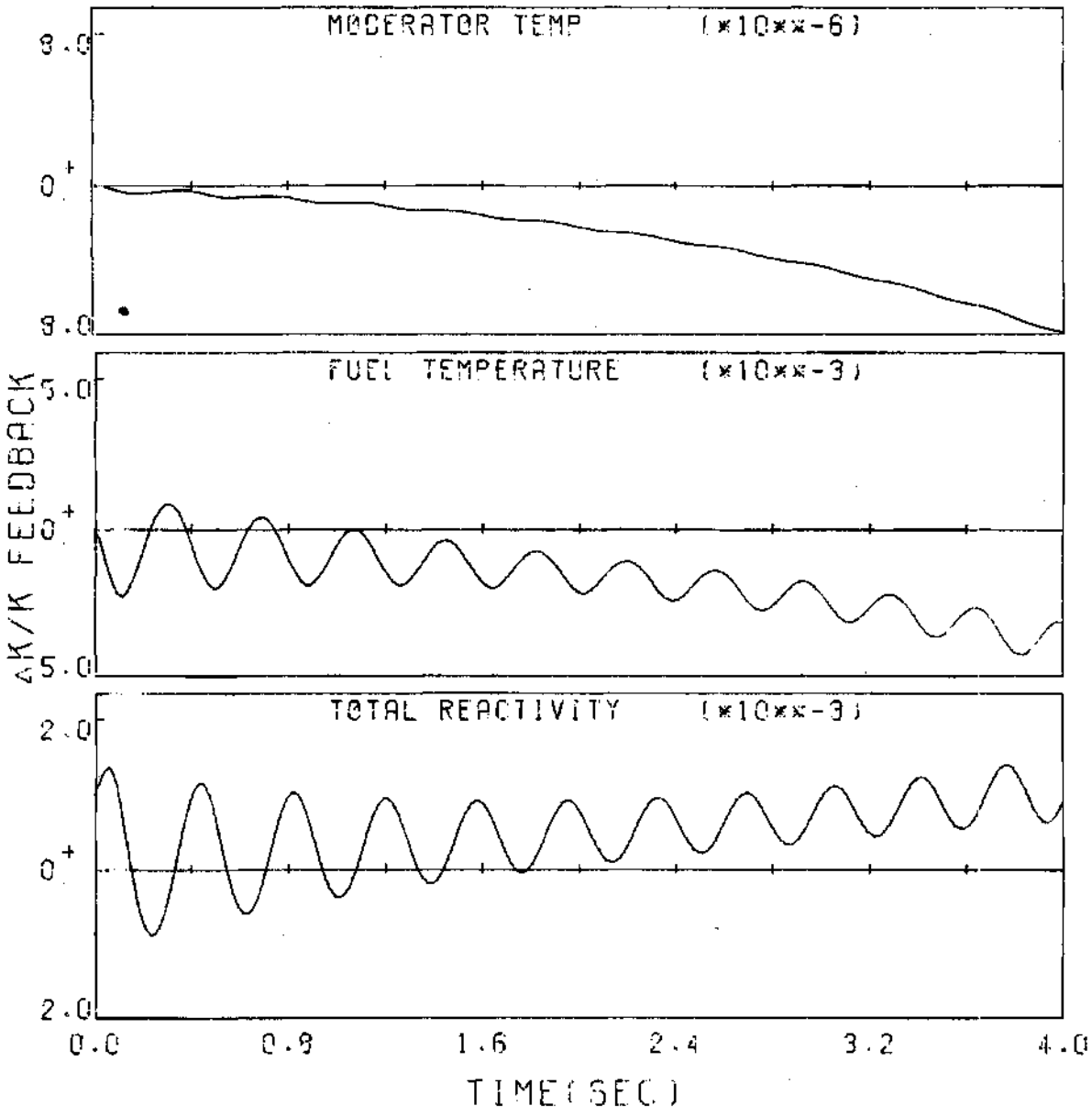

Figure 19. Continued

and insert positive reactivity. The response is thus composed of these oscillations superimposed on the characteristic power increase seen in Figure 7. In this case, the cavity pressure reaches 440 atmospheres about four seconds after the initial reactivity insertion. Thus, if the cavity pressure is the only design constraint, increasing α_{r_f} does not affect the control problem significantly; the large power oscillations may, however, present a problem in protecting the cavity wall from excessive heat fluxes.

A prediction of the system's response to the .1 percent reactivity insertion was made with equation (2-30) modified to be

$$\frac{\dot{m}_{f_e}}{\dot{m}_{p_e}} = \left(\frac{V_f}{V_c}\right)^2 \tag{4-1}$$

The effect of changing the exponent in the above equation from three to two is to increase the predicted amount of fuel loss following an increase in fuel cloud radius. Since the fuel radius increases with an increase in power, additional fuel loss could make the response more sluggish. The results predicted for this case were, however, almost identical to the results of Figure 7; the fuel residence time for the reactor is so long that, even with the above modification, no significant amount of fuel is lost during the time required for the attainment of the critical pressure.

Evaluation of Control Systems

Obviously, any reactor concept whose characteristic response is similar to that indicated in Figure 7 will require some form of control

system capable of limiting the cavity pressure to values which will not risk system damage. The three obvious mechanisms of control arising from the previously discussed results are regulation of fuel injection rate and regulation of the propellant injection rate. Control rods or drums located in the moderator region are also feasible.

Since alterations in the fuel injection rate cause only very slow changes in reactor power, the regulation of the amount of fuel being inserted into the cavity would seem to be an effective control method for very slow transients only. As can be seen from Figure 14, a total shutoff of fuel injection results in a power reduction of five percent after four seconds; since this response is considerably more slow than the power increases predicted for other perturbations, the conclusion may be drawn that the reactor cannot be fully controlled through the use of fuel injection regulation. This assumption is borne out by the results obtained by simultaneously inserting .1 percent positive reactivity and shutting off the fuel inlet; the response in this case was essentially the same as the response for a .1 percent reactivity insertion only.

As mentioned in the discussion of Figures 10 and 12, small changes in the propellant inlet mass flow rate produce large changes in power levels. For this reason, it can be assumed that regulation of the propellant injection rate would be a useful control mechanism. The assumption was tested by increasing the propellant injection rate by 10 percent at 500 milliseconds after a .1 percent reactivity insertion--the result was a reactor shutdown. Further studies indicated that, although regulation of the propellant injection rate can be used to limit power excursions,

the resolution of the resultant control was poor and even small changes in propellant inlet flow rate tended to shut the reactor down.

The use of some type of control drums in the moderator region has been proposed as a mechanism of reactor control for the coaxial flow reactor, and, judging from the above discussion, it would seem that this may be the most advantageous form. Current control systems have response times on the order of 10 milliseconds, and negative reactivity insertions of 60 - 70 percent per second can be achieved. Calculations in which negative reactivity was inserted at this rate as long as two seconds after the insertion of .1 percent positive reactivity indicated that the response could be limited so that the critical pressure was not reached. Thus, it appears that state-of-the-art controls techniques should be adequate to control the coaxial flow gaseous core nuclear reactor.

CHAPTER V

CONCLUSIONS AND RECOMMENDATIONS

Conclusions

The analysis described herein has shown that the work previously done experimentally and theoretically in conjunction with gaseous core reactor steady state analysis combined with elementary heat and mass balances is sufficient to postulate a soluble set of equations which constitute a mathematical model of the coaxial flow gaseous core nuclear reactor in the non-steady state. These equations take the form of a set of 22 first-order differential equations which may be solved by any of several commonly applied numerical techniques.

The system responses predicted for perturbations of system parameters indicate that the reactor is not inherently stable, that is, increases in power are not automatically limited by negative reactivity effects. The feedback reactivity effects do render the reactor's response more sluggish than the response of a system with no feedback. In addition, the time scale for the reactor to reach conditions which might cause system damage is long enough so that present control technology can be invoked to control the reactor.

The model is slightly sensitive to variations in the propellant and fuel temperature coefficients of reactivity and quite sensitive to variations in the propellant density and fuel cloud radius coefficients.

Changes in fuel mass and moderator temperature coefficients have virtually no effect on the model. Changing the rate at which fuel is lost as the fuel volume fraction increases also does not affect the model's predictions.

The best of the proposed control systems seems to be the concept of control drums in the moderator region. Regulation of the fuel injection rate does not give reactivity insertions fast enough to limit most transients, and regulation of the propellant injection rate was found to be good only for shutdown of the reactor--any change in propellant inlet flow rate introduces fairly large changes in reactivity.

Recommendations

Since the neutron density, the fuel and propellant temperatures, and the flow velocities in the reactor cavity are spatially dependent, the predicted dynamics characteristics of the system could change if these variations were taken into account. Of most importance in terms of determining whether system damage occurs during a transient is a calculation of the heat flux to the cavity wall. A knowledge of the temperature and power generation distributions is necessary for this calculation to be made, and, for this reason, it is recommended that further coaxial flow gas-core dynamics models should be derived which include a dynamic calculation of the spatial temperature and power distributions.

The model showed some sensitivity to variations in the values assumed for the reactivity coefficients. An accurate knowledge of these coefficients is, of course, critical to accurate predictions of reactor response, and, since the coefficients cannot be measured until a full-

scale reactor is built, neutronics calculations reflecting the operating conditions of the system should be performed to ascertain the values of the reactivity coefficients. Also, calculations should be performed to find values for the effective delayed neutron fraction by taking the difference in prompt and delayed neutron birth energy into account.

APPENDIX A

LIST OF SYMBOLS

The following is a list of the symbols used in the derivation of the dynamics model presented in Chapter II. Only those parameters which apply to the dynamics model itself are listed to avoid confusion with symbols used in general discussions.

n	average neutron density
C_i	average concentration of the i^{th} delayed neutron precursor
λ_i	i^{th} delayed group decay constant
λ_f	reciprocal of fuel residence time
ℓ	average neutron lifetime
β	delayed neutron fraction
β_{eff}	effective delayed neutron fraction (takes into account only possible loss of precursors from core)
m_f	fuel mass contained in reactor cavity
C_f	specific heat of fuel
T_f	average fuel temperature
m_p	propellant mass contained in reactor cavity
C_p	specific heat of propellant
T_p	average propellant temperature
r_f	fuel cloud radius
A_f	fuel cloud surface area
T_{f_b}	fuel brightness temperature

T_{p_b}	propellant brightness temperature
η	constant used to relate fuel average and brightness temperature
ϵ	constant used to relate propellant average and brightness temperatures
σ	Stefan-Boltzmann constant
P	reactor power
N_f	fuel atom density
σ_f	fuel fission cross section
ϕ	average neutron flux
V_f	fuel cloud volume
v	average neutron velocity
A_v	Avogadro's number
M_f	molecular weight of fuel
γ	constant of proportionality between reactor power and fuel mass and neutron density
$\dot{m}_{f_i}$	fuel mass flow rate at cavity inlet
$\dot{m}_{f_e}$	fuel mass flow rate at cavity exit
$\dot{m}_{p_i}$	propellant mass flow rate at cavity inlet
$\dot{m}_{p_e}$	propellant mass flow rate at cavity exit
h_{p_i}	propellant enthalpy at cavity inlet
h_{p_e}	propellant enthalpy at cavity exit
p	cavity pressure
K	constant of proportionality for choked flow equation
R	constant of proportionality for equation of state of hydrogen
ρ_p	average propellant density
ρ_f	average fuel density

m_m moderator mass

C_m moderator specific heat

T_m average moderator temperature

h_{pc_m} moderator-primary coolant heat transfer coefficient

A_{pc_m} moderator-primary coolant heat transfer area

$\bar{T}_{pc_m}$ average primary coolant temperature in moderator

$T_{pc_{m_e}}$ primary coolant temperature at moderator exit

$T_{pc_{m_i}}$ primary coolant temperature at moderator inlet

$\dot{m}_{pc}$ primary coolant mass flow rate

C_{pc} primary coolant specific heat

m_{pc_m} mass of primary coolant in moderator

$m_{pc_{px}}$ mass of primary coolant in primary heat exchanger

$\bar{T}_{pc_{px}}$ average primary coolant temperature in primary heat exchanger

$T_{pc_{px_e}}$ primary coolant temperature at primary heat exchanger exit

$T_{pc_{px_i}}$ primary coolant temperature at primary heat exchanger inlet

$h_{pc_{px}}$ primary coolant-primary heat exchanger heat transfer coefficient

$A_{pc_{px}}$ primary coolant-primary heat exchanger heat transfer area

C_{px} primary heat exchanger specific heat

m_{px} primary heat exchanger mass

T_{px} average primary heat exchanger temperature

$\bar{T}_{rc_{px}}$ average radiator coolant temperature in primary heat exchanger

$T_{rc_{px_e}}$ radiator coolant temperature at primary heat exchanger exit

$T_{rc_{px_i}}$ radiator coolant temperature at primary heat exchanger inlet

$\bar{T}_{tc_{px}}$ average turbine circuit fluid temperature in primary heat exchanger

$T_{tc_{px_e}}$ turbine circuit fluid temperature at primary heat exchanger exit

$T_{tc_{px_i}}$ turbine circuit fluid temperature at primary heat exchanger inlet

$h_{rc_{px}}$ primary heat exchanger-radiator coolant heat transfer coefficient

$A_{rc_{px}}$ primary heat exchanger-radiator coolant heat transfer area

$h_{tc_{px}}$ primary heat exchanger-turbine circuit fluid heat transfer coefficient

$A_{tc_{px}}$ primary heat exchanger-turbine circuit fluid heat transfer area

$m_{rc_{px}}$ mass of radiator coolant in primary heat exchanger

$m_{tc_{px}}$ mass of turbine circuit fluid in primary heat exchanger

C_{rc} radiator coolant specific heat

C_{tc} turbine circuit fluid specific heat

$\dot{m}_{rc}$ radiator coolant mass flow rate

$\dot{m}_{tc}$ turbine circuit fluid mass flow rate

m_{rc_r} mass of radiator coolant in space radiator

$\bar{T}_{rc_r}$ average temperature of radiator coolant in space radiator

$T_{rc_{r_e}}$ radiator coolant temperature at space radiator

$T_{rc_{r_i}}$ radiator coolant temperature at space radiator inlet

h_{rc_r} radiator coolant-space radiator heat transfer coefficient

A_{rc_r} radiator coolant-space radiator heat transfer area

T_r space radiator temperature

A_r space radiator effective radiating area

m_r mass of space radiator

C_r space radiator specific heat

$\bar{T}_{tc_{pp}}$ average turbine circuit fluid temperature in propellant preheater

$T_{tc_{pp_e}}$ turbine circuit fluid temperature at propellant preheater exit

$T_{tc_{pp_i}}$ turbine circuit fluid temperature at propellant preheater inlet

$h_{tc_{pp}}$ propellant preheater-turbine circuit fluid heat transfer coefficient

$A_{tc_{pp}}$ propellant preheater-turbine circuit fluid heat transfer area

$m_{tc_{pp}}$ mass of turbine circuit fluid in propellant preheater

T_{pp} average propellant preheater temperature

m_{pp} propellant preheater mass

C_{pp} propellant preheater specific heat

$\bar{T}_{p_{pp}}$ average propellant temperature in propellant preheater

$T_{p_{pp_e}}$ propellant temperature at propellant preheater exit

$T_{p_{pp_i}}$ propellant temperature at propellant preheater inlet

$m_{p_{pp}}$ propellant mass in propellant preheater

$h_{p_{pp}}$ propellant-propellant preheater heat transfer coefficient

$A_{p_{pp}}$ propellant-propellant preheater heat transfer area

$\dot{m}_{p_{pp}}$ mass flow rate of propellant through propellant preheater

$h_{p_{pp_e}}$ propellant enthalpy at propellant preheater exit

$h_{p_{pp_i}}$ propellant enthalpy at propellant preheater inlet

APPENDIX B

CALCULATION OF THE STEADY STATE FUEL-TO-PROPELLANT AND PROPELLANT-TO-FUEL HEAT RADIATION RATES

As mentioned in the text, Williams and Byrn[37] have calculated the volumetric heat deposition in the propellant as a function of the distance from the fuel cloud edge for core conditions approximating those of a gaseous core reactor at steady state. The general heat deposition curve, shown in Figure 20, does not change shape for values of power input which do not cause significant changes in the propellant absorption coefficient. Thus, $Q(x)/Q_o$, where $Q(x)$ is the local heat deposition rate at distance x from the fuel and Q_o is the heat deposition rate at the fuel cloud edge, does not change with different values of Q_o.

For this analysis, the propellant region is discretized into 10 regions; these regions have the shape of spherical shells, and they are concentric with the spherical fuel cloud. The heat deposition plot is thus approximated by a histogram of the average values of the volumetric heat source in each region. In light of the discussion above, the values for the average heat deposition in each region can be replaced by (Q_i/Q_1) where Q_i is the heat deposition in the i^{th} region and Q_1 is the heat deposition rate in the first region. The region boundaries and the fractional heat deposition rates are listed in Table 6.

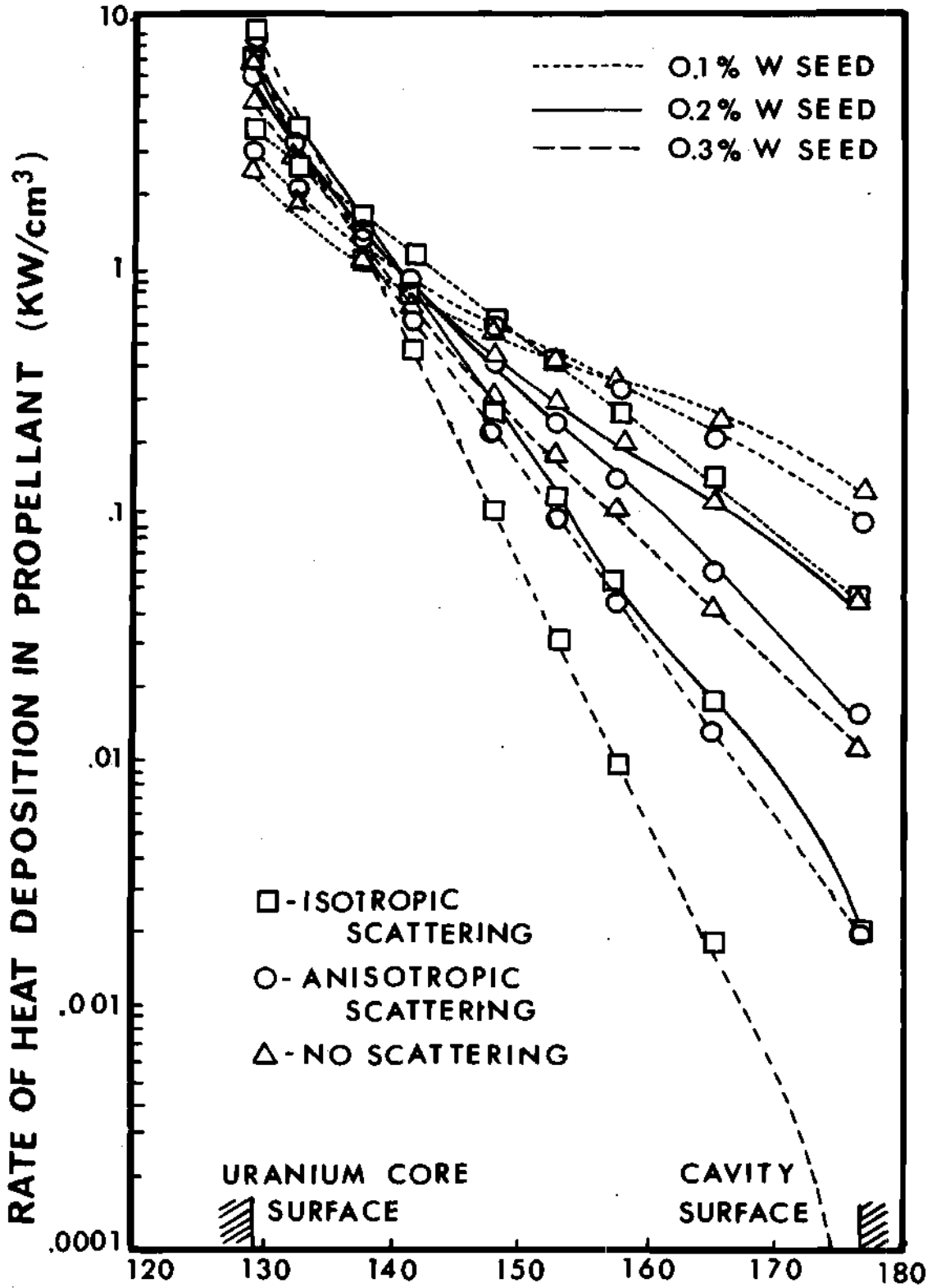

Figure 20. Rate of Heat Deposition in the Propellant Region versus Distance from the Fuel Cloud Surface

Table 6. Data for Definition of the Regions Used in Calculating the Steady State Propellant-to-Fuel and Fuel-to-Propellant Heat Fluxes

Region	r_{inner}(ft)	r_{outer}(ft)	Q_i/Q_1
1	3.35	3.515	1.0
2	3.515	3.68	.6786
3	3.68	3.845	.3214
4	3.845	4.01	.1714
5	4.01	4.175	.0929
6	4.175	4.34	.05
7	4.34	4.505	.0268
8	4.505	4.67	.0118
9	4.67	4.835	.0086
10	4.835	5.00	.0054

Since the assumption is being made that all of the thermal radiation emitted from the fuel is absorbed in the propellant, the total heat deposition rate in the propellant must be equal to the rate of heat emission from the fuel. Letting $a_i = (Q_i/Q_1)$, the total heat transfer rate is given by

$$Q_{fuel\text{-}prop} = Q_1V_1 + a_2V_2Q_1 + \ldots + a_{10}V_{10}Q_1 \qquad \text{(A-1)}$$

Once the heat deposition rates are known for each region, the steady state values of propellant-to-fuel and fuel-to-propellant heat fluxes can be found from a knowledge of the core geometry and the absorption coefficient of the propellant. The approach taken here is to determine the fraction of radiation which is absorbed at a single point in each region, reemitted, and reabsorbed in the fuel region. Figure 21 serves as a description of the relevant geometry and defines the coordinate system used in the analysis.

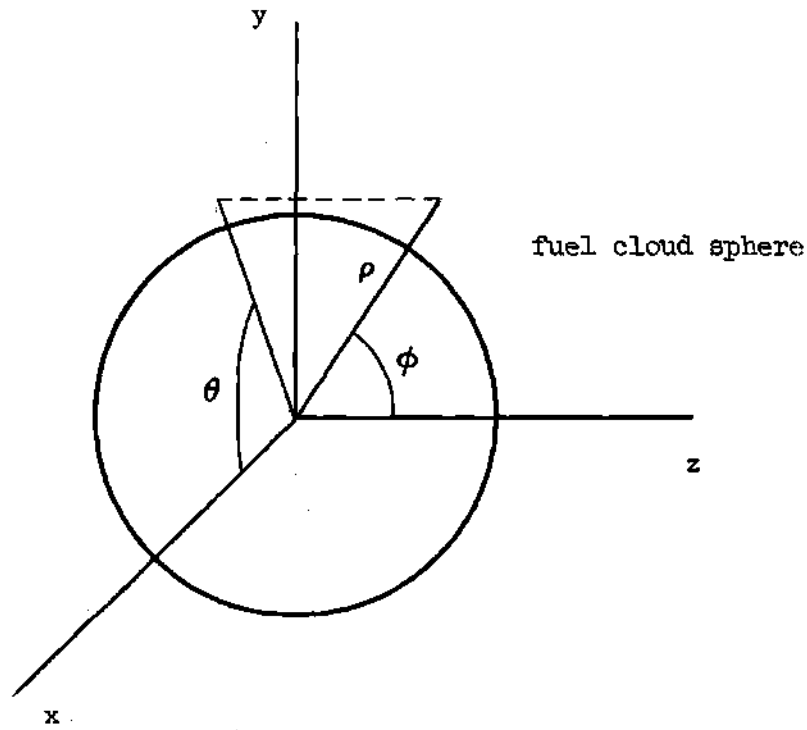

Figure 21. Definition of the Coordinate System Used in Deriving the Steady State Propellant-to-Fuel and Fuel-to-Propellant Radiant Heat Fluxes

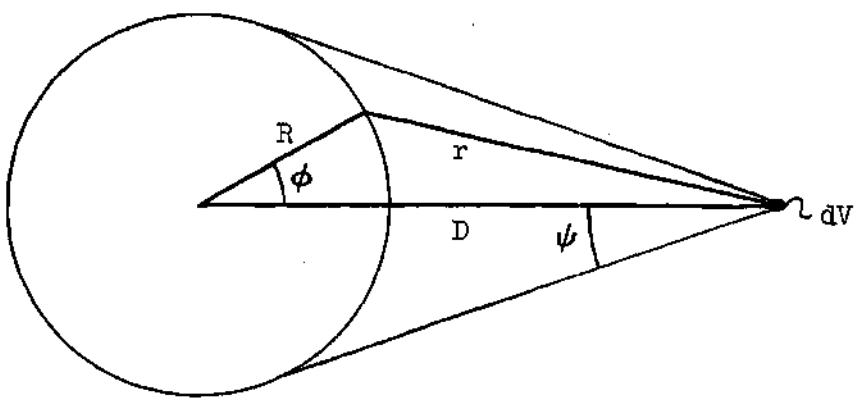

Figure 22. Geometrical Configuration Used to Find the Distance from a Point in the Propellant to the Fuel Cloud Surface

Since the reactor is considered to be at steady state and the temperature at each point is constant, the heat radiated at each point in the propellant must be equal to the heat deposited at that point. Consider, then, a differential volume dV located in region i; the dimensions of dV are assumed to be very small in comparison with the cavity dimensions. The total amount of radiation emitted in dV is $Q_i dV$. Since dV is vanishingly small, the radiant heat flux at distance r from dV in the propellant is given by

$$q = \frac{Q_i dV\, e^{-kr}}{4\pi r^2} \tag{A-2}$$

where k is the propellant absorption coefficient. The assumption is made, of course, that the radiation is emitted isotropically from each point.

From the geometry of Figure 21 it is obvious that, if scattering is neglected, only that radiation emitted from dV at an angle of less than ψ (see Figure 22) from the z-axis can possibly intersect the fuel cloud. The amount of heat emitted in dV which enters the fuel cloud is thus given by the integral of the flux over the fuel surface lying inside the cone generated by rotating a line drawn at the angle ψ around the z-axis. The heat to the fuel from dV is, then,

$$Q_{\text{from dV}} = \int_A \int \frac{Q_i dV\, e^{-kr}}{4\pi r^2}\, dA \tag{A-3}$$

The total amount of heat reradiated to the fuel from region i is given by

$$Q_{rerad_i} = \int_{V_i} \int_A \int \frac{Q_i \, e^{-kr}}{4\pi \, r^2} \, dA \, dV \qquad (A\text{-}4)$$

Now, since the width of the regions is small in comparison with the cavity dimensions, no significant error is introduced by assuming that all of the radiant energy emitted in the region is emitted in a spherical shell of thickness dr located at the center of the region. The volumetric energy density must, of course, be higher in this shell so the total energy deposited in each region is the same. Denoting the volume of the spherical shell of differential thickness by V_i', equation (A-4) becomes

$$Q_{rerad_i} = \int_{V_i'} \int_A \int \frac{Q_i' \, e^{-kr}}{4\pi \, r^2} \, dA \, dV \qquad (A\text{-}5)$$

where Q_i' is the appropriately increased heat deposition. The integrand of equation (A-5) does not change appreciably over V_i' so the surface integral may be brought out of the volume integral. Combining this operation with performing the volume integration yields

$$Q_{rerad_i} = Q_{dep_i} \int_A \int \frac{e^{-kr}}{4\pi \, r^2} \, dA \qquad (A\text{-}6)$$

where Q_{dep_i} is the total heat deposited in region i.

Since the problem yields itself to analysis using a spherical coordinate system, dA may be written

$$dA = R^2 \sin\phi \, d\theta \, d\phi; \qquad (A\text{-}7)$$

dA naturally lies on the surface of the fuel cloud. Denoting the angle between the z-axis and the tangent to the fuel cloud surface drawn through the centerline of region i by ψ_i and inserting the appropriate limits on the integral of equation (A-6) yields

$$Q_{rerad_i} = Q_{dep_i} R^2 \int_0^{2\pi} \int_{-\psi_i}^{\psi_i} \frac{e^{-kr} \sin\phi}{4\pi r^2} \, d\phi \, d\theta \qquad \text{(A-8)}$$

Before the integral of equation (A-8) can be evaluated, r must be expressed in terms of the coordinates ρ, θ, and ϕ. The desired relation may be easily derived by examining the geometry of Figure 22. The Law of Cosines applied to the triangle formed by the lines denoted as R, r, and D_i gives

$$r = \sqrt{R^2 + D_i^2 - 2D_i R\cos\phi} \qquad \text{(A-9)}$$

Substituting the relation for r into equation (A-8) and noting that the integrand does not depend on θ allows the rewriting of (A-7) to give

$$Q_{rerad_i} = \frac{Q_{dep_i} R^2}{2} \int_{-\psi}^{\psi} \frac{\sin\phi \, e^{-k\sqrt{R^2 + D_i^2 - 2D_i R\cos\phi}}}{R^2 + D_i^2 - 2D_i R\cos\phi} \, d\phi \qquad \text{(A-10)}$$

The integral of equation (A-10) was evaluated numerically for each region.

The knowledge of the reradiated heat from each region which is incident on the fuel cloud allows the calculation of the total propellant-to-fuel heat radiation rate by simply adding the reradiation rates for all the regions. Thus

$$Q_{\text{propellant-to-fuel}} = \sum_i Q_{\text{rerad}_i} \qquad \text{(A-11)}$$

Armed with the above knowledge, the calculation of the actual values of the heat transfer rates proceeds as follows. The net rate of heat transfer from the fuel to the propellant Q_{net} is known from the specifications of the reference system to be 5550 MW. The propellant-to-fuel heat transfer rate $Q_{\text{prop-fuel}}$ is then assumed to be some fraction of Q_{net} so that

$$Q_{\text{fuel-prop}} = Q_{net} + Q_{\text{prop-fuel}}.$$

Q_1 can then be found from equation (A-1), and the remainder of the Q_i's can be found by use of Table 6. A check value of $Q_{\text{prop-fuel}}$ can then be calculated from equation (A-11); if the assumed and calculated values for $Q_{\text{prop-fuel}}$ do not agree, the entire process is repeated using different assumed values until convergence occurs.

Execution of the procedure described above indicates that the steady state value of the propellant-to-fuel heat transfer rate is about 3.6 percent of Q_{net}. η and ϵ can be found from the relations

$$\sigma \eta A_f T_f^4 = Q_{\text{fuel-prop}}$$

$$\sigma \epsilon A_f T_p^4 = Q_{\text{prop-fuel}}$$

to be 6.18×10^{-3} and 1.24×10^{-3}, respectively.

APPENDIX C

In order to apply the numerical techniques discussed in Chapter III, it is necessary to rearrange equation (2-27) so that no term containing $\frac{dp}{dt}$ appears on the left-hand side.

The first operation required is to insert the suggested expression for ρ_p into $\frac{d\rho_p}{dt}$ which yields

$$\frac{d\rho_p}{dt} = \frac{d}{dt}\left[\frac{m_p}{(V_c - m_f/\rho_f)}\right] \tag{A-12}$$

which, in turn, can be expanded to give

$$\frac{d\rho_p}{dt} = \frac{1}{V_p}\frac{dm_p}{dt} + \frac{\rho_p}{V_p}\left(\frac{1}{\rho_f}\frac{dm_f}{dt} - \frac{V_f}{\rho_f}\frac{d\rho_f}{dt}\right) \tag{A-13}$$

where

$$V_p = (V_c - m_f/\rho_f) \tag{A-14}$$

and

$$V_f = m_f/\rho_f \tag{A-15}$$

Inserting the expression given in equation (2-29) of the text for $\frac{d\rho_f}{dt}$ into (A-13) and expanding yields

$$\frac{d\rho_p}{dt} = \frac{1}{V_p}\frac{dm_p}{dt} + \frac{\rho_p}{V_p\rho_f}\frac{dm_f}{dt} - \frac{S\rho_p V_f T_f^{-1.77}}{V_p\rho_f}\frac{dp}{dt} \qquad \text{(A-16)}$$

$$+ \frac{1.77S\rho_p V_f T_f^{-2.77p}}{V_p\rho_f}\frac{dT_f}{dt}$$

Substituting equation (A-16) for $\frac{d\rho_p}{dt}$

$$\frac{dp}{dt} = \frac{1.6p}{T_p}\frac{dT_p}{dt} + \frac{RT_p^{1.6}}{V_p}\frac{dm_p}{dt} + \frac{R\rho_p T_p^{1.6}}{V_p\rho_f}\frac{dm_f}{dt} \qquad \text{(A-17)}$$

$$- \frac{V_f RT_p^{1.6}\rho_p ST_f^{-1.77}}{V_p\rho_f}\frac{dp}{dt} + \frac{1.77V_f S_p T_f^{-2.77}R\rho_p T_p^{1.6}}{V_p\rho_f}\frac{dT_f}{dt}$$

Recalling that

$$p = R\,T^{1.6}\,\rho_p \qquad \text{(A-18)}$$

and that

$$\rho_f = S\,p\,T_f^{-1.77} \qquad \text{(A-19)}$$

allows the reduction of equation (A-17) to yield

$$\frac{dp}{dt} = \frac{1.6p}{T_p}\frac{dT_p}{dt} + \frac{RT_p^{1.6}}{V_p}\frac{dm_p}{dt} + \frac{p}{V_p\rho_f}\frac{dm_f}{dt} - \frac{V_f}{V_p}\frac{dp}{dt} \qquad \text{(A-20)}$$

$$- \frac{V_f}{V_p}\frac{dp}{dt} + \frac{1.77V_f p}{V_p T_f^{1.77}}\frac{dT_f}{dt}$$

Finally, rearranging equation (A-20) so that all terms containing $\frac{dp}{dt}$ appear on the left-hand side yields

$$\left(1 + \frac{V_f}{V_p}\right) \frac{dp}{dt} = \frac{1.6p}{T_p} \frac{dT_p}{dt} + \frac{RT_p^{1.6}}{V_p} \frac{dm_p}{dt} + \frac{p}{V_p \rho_f} \frac{dm_f}{dt} + \frac{1.77 V_f p}{V_p T_f^{1.77}} \frac{}{dt} \qquad \text{(A-21)}$$

which is the desired result.

BIBLIOGRAPHY

1. Clement, J. D. and Williams, J. R., "Gas-Core Reactor Technology," Reactor Technology, 13, No. 1, 13-15 (July 1970).

2. Bussard, P. W. and DeLauer, R. D., Fundamentals of Nuclear Flight, McGraw-Hill Book Company, New York, 1965.

3. Ragsdale, R. G., Personal Communication, May 1970.

4. Rom, F. E., "Gaseous Nuclear Rocket," Patent No. 3,202,582, filed August 28, 1961.

5. Ragsdale, R. G., "Are Gas-Core Nuclear Rockets Attainable?" AIAA Paper No. 68-570, June 1968.

6. Ragsdale, R. G., "Relationship Between Engine Parameter and the Fuel Mass Contained in an Open-Cycle Gas-Core Reactor," NASA-TM-X-52733, January 1970.

7. McLafferty, G. H., "Gaseous Reactor Container," Patent No. 3,223, 591, filed August 27, 1962.

8. McLafferty, G. H., "Investigation of Gaseous Nuclear Rocket Technology," Summary Technical Report, United Aircraft Research Laboratories Report No. H-910093-46, November 1969.

9. Clark, J. W., Johnson, B. V., Kendall, J. L., Mansing, A. E., and Travers, A., "Open Cycle and Light-Bulb Types of Vortex-Stabilized Gaseous Nuclear Rockets," Journal of Spacecraft and Rockets, 5(8), 941 (August 1968).

10. Rosa, R. J., Magnetohydrodynamic Energy Conversion, McGraw-Hill Book Company, New York, 1968.

11. Sherman, A., "Gaseous Fission Closed Loop MHD Generator," Proceedings of the Symposium on Research on Uranium Plasmas and Their Technological Applications, University of Florida, January 1970.

12. Rosa, R. J., "Propulsion System Using a Cavity Reactor and Magnetohydrodynamic Generator," American Rocket Society Journal, July 1961.

13. Williams, J. R. and Shelton, S. V., "Gas Core Reactors for MHD Power Systems," Proceedings of the Symposium on Research on Uranium Plasmas and Their Technological Applications, University of Florida, January 1970.

BIBLIOGRAPHY (Continued)

14. Williams, J. R., Kallfelz, J. M., and Shelton, S. V., "A Parametric Survey of Gas-Core Reactor-MHD Power Plant Concepts," Proceedings of the Intersociety Energy Conversion Engineering Conference, Las Vegas, Nevada, September 1970.

15. Kallfelz, J. M. and Williams, J. R., "Exploratory Calculations for a Gaseous Core Fast Breeder Reactor," ANS Transactions 14, No. 1, November 1970.

16. Esposito, V. J., "The Transient and Steady State Dynamics of a Nuclear Rocket Engine," Ph.D. Thesis, University of Virginia, August 1968.

17. Latham, T. S., Bauer, H. E., and Rodgers, R. J., "Studies of Nuclear Light Bulb Start-Up Conditions and Engine Dynamics," United Aircraft Research Laboratories Report No. H-910375-4, September 1969.

18. Bauer, H. E., Rodgers, R. J., and Latham, T. S., "Analytical Studies of Start-Up and Dynamic Response Characteristics of the Nuclear Light Bulb Engine," United Aircraft Research Laboratories Report No. J-910900-5, September 1970.

19. McLafferty, G. H. and Bauer, H. E., "Studies of Specific Nuclear Light Bulb and Open-Cycle Vortex-Stabilized Gaseous Nuclear Rocket Engines," United Aircraft Research Laboratories Report No. F-910093-37, September 1967.

20. McLafferty, G. H., "Absorption of Thermal Radiation in the Transparent Wall of a Nuclear Light Bulb Rocket Engine," Journal of Spacecraft and Rockets, 4(6), 1967.

21. Smith, H. P., Jr. and Stenning, A. H., "Open Loop Stability and Response of Nuclear Rocket Engines," Nuclear Science and Engineering, 11 (1961).

22. Latham, T. S., "Nuclear Studies of the Nuclear Light-Bulb Rocket Engine," NASA-CR-1030, September 1967.

23. Pincock, G. D. and Kunze, J. F., "Cavity Reactor Critical Experiment, Volume I," General Electric Company, NASA-CR-72550, September 1967.

24. Pincock, G. D. and Kunze, J. F., "Cavity Reactor Critical Experiment, Volume II," General Electric Company, NASA-CR-72550, May 1968.

BIBLIOGRAPHY (Continued)

25. Pincock, G. D. and Kunze, J. F., "Cavity Reactor Critical Experiment, Volume III," General Electric Company, NASA-CR-72550, September 1968.

26. Pincock, G. D. and Kunze, J. F., "Cavity Reactor Critical Experiment, Volume IV," General Electric Company, NASA-CR-72550, May 1969.

27. Pincock, G. D. and Kunze, J. F., "Cavity Reactor Critical Experiment, Volume V," General Electric Company, NASA-CR-72550, November 1969.

28. Kascak, A. F., "Estimates of Local and Average Fuel Temperatures in a Gaseous Nuclear Rocket Engine," NASA-TN-D-4164, 1967.

29. Kascak, A. F., "The Radiant Heat Flux Limit of By-Pass Flow in a Uranium Plasma Rocket," NASA-TM-X-52739, January 1970.

30. Hyland, R. E., "Evaluation of Critical Mass for Open-Cycle Gas-Core Rocket Reactors," NASA-TM-X-52820, June 1970.

31. Lanzo, C. D., "A Flow Experiment on a Curved-Porous-Wall Gas-Core Reactor Geometry," NASA-TM-X-1852, 1969.

32. Johnson, B. V., "Exploratory Experimental Study of the Effects of Inlet Conditions on the Flow and Containment Characteristics of Coaxial Flows," United Aircraft Research Laboratories Report No. H-910091-21, September 1969.

33. Ragsdale, R. G. and Kascak, A. F., "Simple Equations for Calculating Temperature Distributions in Radiating Gray Gases," NASA-TN-D-5226, 1969.

34. Parks, D. E., Lane, G., Stewart, J. C., and Peyton, S., "Optical Constants of Uranium Plasma," Report GA-8244, Gulf General Atomic, NASA-CR-72348, February 1968.

35. Kascak, A. F., "Coaxial Flow Radiant Heat Transfer Analysis," Proceedings of an Advanced Nuclear Propulsion Symposium, LA-3229-MS, Los Alamos Scientific Laboratory, 1965.

36. Patch, R. W., "Thermodynamic Properties and Theoretical Rocket Performance of Hydrogen to 100,000 °K and 1000 Atmospheres," NASA-Lewis Technical Note E-6172, 1971.

BIBLIOGRAPHY (Concluded)

37. Williams, J. R., Byrn, N. R., Clement, J. D., and Jacobs, W. R., "Monte Carlo Radiant Heat Transfer Analysis of Gas Core Reactors," ANS Transactions, 13, No. 1, pp. 13-15 (July 1970).

38. Shapiro, A. H., The Dynamics and Thermodynamics of Compressible Fluid Flow, Volume 1, Ronald Press, New York, 1953.

39. Rust, J. H., Personal Communication, June 1971.

40. Hyland, R. E., Personal Communication, March 1971.

41. James, M. L., Smith, G. M., and Wolford, J. C., Applied Numerical Methods for Digital Computation with FORTRAN, International Textbook Company, Scranton, Pa., 1967.

VITA

Kyle Hugh Turner, Jr. was born on September 19, 1946 in Atlanta, Georgia, where, in 1964, he graduated from Henry Grady High School. In 1968, he received his Bachelor of Electrical Engineering degree from the Georgia Institute of Technology. Mr. Turner entered graduate school at the Georgia Institute of Technology in 1968 and completed his Master of Science in Nuclear Engineering in 1969.

In 1969, Mr. Turner began investigating the dynamics properties of gaseous core nuclear reactors. He is co-author of "A Dynamics Model of the Coaxial Flow Gaseous Core Nuclear Reactor," published in the Transactions of the American Nuclear Society. He has also had a paper accepted for presentation at the 2nd Symposium on Uranium Plasmas: Research and Applications, November 15-17, 1971 at the Georgia Institute of Technology.

Mr. Turner is a member of the American Nuclear Society, the Association for Computing Machinery, Sigma Xi, and Eta Kappa Nu.